Decellularized Liver Nanofibers Enhance and Stabilize the Long-term Functions of Primary Human Hepatocytes In Vitro

Jennifer S. Liu[1†], Liszt Y. C. Madruga[2†], Yang Yuan[1], Matt J. Kipper[2*], and Salman R. Khetani[1*]

[1]Department of Biomedical Engineering, University of Illinois at Chicago, Chicago, IL

[2]Department of Chemical & Biological Engineering, Colorado State University, Fort Collins, CO

† Authors contributed equally
* Co-corresponding authors

[1] Department of Biomedical Engineering
University of Illinois at Chicago
851 South Morgan Street
Chicago, Illinois, 60607, USA

[2]Department of Chemical and Biological Engineering
Colorado State University
1370 Campus Delivery
Fort Collins, CO, 80523, USA

*Co-corresponding authors: skhetani@uic.edu; Matthew.Kipper@ColoState.EDU

Keywords: Electrospinning, Co-cultures, 3T3-J2 fibroblasts, Porcine liver, collagen

Abstract

Owing to significant differences across species in liver functions, *in vitro* human liver models are used for screening the metabolism and toxicity of compounds, modeling diseases, and cell-based therapies. However, the extracellular matrix (ECM) scaffold used for such models often does not mimic either the complex composition or the nanofibrous topography of native liver ECM. Thus, here we develop novel methods to electrospin decellularized porcine liver ECM (PLECM) and collagen I into nano- and microfibers (~200-1000nm) without synthetic polymer blends. Primary human hepatocytes (PHHs) on nanofibers in monoculture or in co-culture with non-parenchymal cells (3T3-J2 embryonic fibroblasts or primary human liver endothelial cells) display higher albumin secretion, urea synthesis, and cytochrome-P450 1A2, 2A6, 2C9, and 3A4 enzyme activities than on conventionally adsorbed ECM controls. PHH functions are highest on the collagen/PLECM blended nanofibers (up to 34-fold higher CYP3A4 activity relative to adsorbed ECM) for nearly 7 weeks in the presence of the fibroblasts. In conclusion, we show for the first time that ECM composition and topography synergize to enhance and stabilize PHH functions for several weeks *in vitro*. Our nanofiber platform could prove useful for the above applications and to elucidate cell-ECM interactions in the human liver.

1. Introduction

Owing to significant differences across species in liver pathways, *in vitro* human liver models are utilized for screening the metabolism and toxicity of pharmaceuticals and industrial chemicals, mimicking the key aspects of liver diseases for the discovery of novel molecular targets, and building tissue surrogates for implantation into patients suffering from end-stage liver failure [1, 2]. Primary human hepatocytes (PHHs) are often used to fabricate such models given their ability to perform the majority of liver functions such as protein synthesis, bile production, glucose and fatty acid metabolism, and the detoxification of endogenous and exogenous substances. However, PHHs rapidly lose phenotypic functions when cultured on their own on extracellular matrix (ECM) proteins (i.e., collagen I) adsorbed onto non-physiological stiff substrates, such as glass and polystyrene [3]. While the PHH phenotype can be stabilized in vitro for several weeks upon co-cultivation with specific non-parenchymal cell (NPC) types, such as stromal fibroblasts, functions still remain below those in freshly isolated PHHs, partly due to the use of non-physiologic substrates [4]. Thus, there remains a critical need to develop more physiologic substrates for PHH and PHH/NPC co-cultures alike.

The liver's ECM is composed of diverse proteins such as collagens, glycoproteins, and proteoglycans [5]. A few attempts have been made at culturing PHHs within ECM that better

mimics *in vivo*-like architecture and/or composition than collagen I adsorbed onto stiff substrates. For instance, sandwiching hepatocytes within two layers of gelled collagen I can induce the reformation of bile canaliculi between adjacent hepatocytes, but other functions, such as drug metabolism enzyme activities, still show a rapid decline [6]. Similarly, culturing hepatocytes with tumor-derived murine Matrigel™ can induce some functions for ~1 week [7], but extrapolating the results using Matrigel to the effects of native liver ECM on hepatic functions is challenging. In contrast, culturing PHHs on decellularized human liver ECM can also transiently improve phenotypic functions [8]; however, such ECM is typically variable in quality due to the unpredictable conditions of the transplant-rejected human livers [9]. We previously found that ECM protein composition can significantly modulate PHH functions on polyacrylamide substrates of liver-like stiffnesses in unexpected ways, but drug metabolism capacity of the cells still declined over time [10], partly because the substrates did not mimic the full protein composition nor the topography of liver ECM. Thus, more *in vivo*-like ECM substrates are needed to induce high and stable PHH functions for several weeks *in vitro*.

In contrast to adsorbed (2-dimensional) ECM, porous 3-dimensional (3D) nanofibrous scaffolds more accurately recapitulate many features of the ECM *in vivo* [11]. Electrospun nanofibrous scaffolds from natural and synthetic materials can improve the phenotype of different cell types, including primary rat hepatocytes [12-15]. The large surface area of

nanofiber matrices can also be used to present a high density of receptor ligands that improve hepatocyte function, including small molecules (e.g. galactose) [16] and proteins (e.g. collagen) [12]. Others have cultured transformed human hepatocyte cell lines on electrospun nanofibers made using blends of polycaprolactone (PCL), collagen, and silk [17] or poly (lactic-*co*-glycolic acid) (PLGA)-based fibers coated with collagen-I or fibronectin [18] and shown improvements in hepatic phenotype relative to non-fibrous substrates. While the above studies demonstrate the utility of nanofibrous scaffolds for liver culture, they are either limited to synthetic fibers that do not adequately mimic the biochemistry of natural liver ECM and/or cell sources such as transformed cell lines and animal-derived hepatocytes that are known to deviate considerably from human liver functions [1, 2]. Thus, there remains a need to develop nanofibrous scaffolds from natural liver ECM that can support the long-term functions of PHHs.

Here, we sought to test the novel hypothesis that PHH monocultures and PHH/NPC co-cultures will display significantly higher liver functions for several weeks on nanofibrous scaffolds fabricated using ECM proteins found in the liver. Towards testing this hypothesis, we first developed novel methods to electrospin stable nanofibers of decellularized porcine liver ECM (PLECM) given the robust availability of healthy porcine livers and the ability of porcine liver ECM to support some rat hepatocyte functions *in vitro* [19]; as control ECM, we utilized rat tail collagen-I and the polysaccharide chitosan. Rat tail collagen-I is widely used for PHH

culture due to its ready availability and cost-effectiveness. Chitosan, has been previously shown to stabilize collagen scaffolds [20, 21] and support some rat hepatocyte functions *in vitro* [15, 22]. We then cultured PHHs on their own and with well-established NPC types [1], namely 3T3-J2 murine embryonic fibroblasts and primary human liver sinusoidal endothelial cells (LSECs), on the different nanofibrous scaffolds and non-fibrous (i.e., adsorbed) control substrates; cell morphology, viability, immunostaining patterns, and phenotypic functions (albumin and urea secretions, and cytochrome-P450 1A2, 2A6, 2C9, and 3A4 enzyme activities) were assessed for up to 47 days in culture.

2. Materials and methods

2.1. ECM fiber fabrication

Procedures for collagen I extraction from rat tails and porcine liver decellularization are detailed in **Supplemental Material** and the pictures and process of porcine liver decellularization are provided in **Supplemental Figure 1**. The solvent 1,1,1,3,3,3-hexafluoro-2-propanol (HFIP) was used to dissolve collagen and PLECM blends overnight under constant stirring, while trifluoroacetic acid (TFA) was used to dissolve chitosan-only solutions; concentrations are provided in **Supplemental Table 1**. Viscosity measurements of the

solutions were taken with a TL7 spindle on a Fungilab (Hauppauge, NY) viscometer at 100 rpm. A glass syringe (Fortuna Optima, Luer lock tip style) containing the macromolecule solution was then placed in a Kent Scientific Genie Plus syringe pump (Torrington, CT) and the solutions were pumped (0.5 to 1.0 mL/hour) for 5+ hours. A high-voltage DC power supply (operated at 15 to 20 kV) (Gamma High Voltage Research, Ormond Beach, FL) was used to create an electric field between a 19-gauge needle and a grounded copper collection plate covered with aluminum foil. Siliconized round glass coverslips (12 mm diameter, Hampton research, Aliso Viejo, CA) were oxidized via oxygen plasma for 5 minutes to facilitate nanofiber attachment [23, 24] and then attached to the aluminum foil using copper tape. The distance of the tip of the needle to the siliconized round glass cover slides was fixed at 15 cm for all conditions [25, 26]. Electrospinning was then conducted at 20 ± 2 °C and 19% relative humidity; viscosities and electrospinning conditions for each macromolecule solution are provided in **Supplemental Table 2.**

Nanofibers that were adhered to the coverslips were crosslinked at room temperature (RT) for 24 hours using a mixture of 1-ethyl-3-(3-dimethyl aminopropyl)carbodiimide (EDC, 20 mM) and *N*-hydroxysuccinimide (NHS, 10 mM) in 90% ethanol [27-29] for all nanofibers except for the chitosan-only nanofibers that were crosslinked with a vapor of 25% glutaraldehyde in water. Lastly, the nanofibers were washed several times with sterile deionized water (obtained from

a Milli-Q water purification system) and kept at 4°C until further use. The process described above is shown schematically in **Figure 1**.

To generate control substrates, O_2 plasma-treated glass coverslips were incubated for 2 hours in 100 µg/mL of either collagen I dissolved in 0.01 N acetic acid or PLECM dissolved in 0.02 N hydrochloric acid. Following two rinses with double-distilled water (ddH_2O), the coverslips were sterilized with 70% (v/v) ethanol in ddH_2O for 1 hour and finally rinsed three times with sterile ddH_2O.

2.2. ECM fiber characterization

Nanofibers were characterized via Fourier transform infrared spectroscopy using attenuated total reflection (FTIR-ATR, Thermo Smart Orbit mounted on a Thermo 8700 spectrometer) with a diamond crystal using a wavelength range of 4000 to 500 cm^{-1} at 4 cm^{-1} resolution and cumulation of 64 scans [30]. The spectra of the nanofibers were compared to the spectra of their pure components. Additionally, nanofibers were coated with 15 nm of gold and observed using a JSM-6500F JEOL Scanning Electron Microscope (SEM, Tokyo, Japan) at an accelerating voltage of 15 kV. The chemical composition of the nanofibers was characterized by X-ray photoelectron spectroscopy (XPS, 5800 spectrometer, Physical Electronics,

Chanhassen, MN). Survey spectra were collected for all nanofibers from 0 to 1100 eV, with a pass energy of 187 eV. High-resolution spectra of the C1s peak were acquired with 0.1 eV steps and an X-ray spot of 800 μm. Origin and Multipak software were used for performing the curve fitting of all presented spectra. The C1s peak (284.8 eV) was used as a reference peak. Nanofiber spectra were compared to the spectra of their respective pure components. Porosity and pore size of the fibers were measured from the SEM images with the aid of ImageJ DiameterJ software using 5 different pictures and the results are shown in **Supplemental Table 3**. Mechanical properties of the nanofibers were measured using an Instron 4442 (Norwood, MA) tensile tester ($n \geq 3$) and results are shown in **Supplemental Table 4**.

2.3. NPC culture

Primary human liver sinusoidal endothelial cells (LSECs, Cell Systems, Kirkland, WA) were passaged up to 14 times using 0.05% trypsin-EDTA (Corning, Manassas, VA) in tissue culture flasks coated with 2 μg/cm^2 fibronectin (Corning); cells were cultured in EGM™-2 Endothelial Cell Growth Medium-2 BulletKit™ (Lonza, Williamsport, PA). The 3T3-J2 murine embryonic fibroblasts, a gift from Howard Green (Harvard Medical School), were passaged up to 11 times using 0.25% trypsin-EDTA (Corning) in tissue culture flasks with medium containing high glucose Dulbecco's Modified Eagle Medium (DMEM) base (Corning) containing 10% (v/v)

bovine calf serum and 1% (v/v) penicillin-streptomycin (Corning).

2.4. PHH monocultures and PHH/NPC co-cultures

Nanofibers adhered to coverslips and adsorbed ECM control coverslips were rinsed once with 1× phosphate buffered saline (PBS, Corning) and incubated overnight in phenol red-free high glucose DMEM (Cytiva, Marlborough, MA) containing 10% bovine calf serum and 1% penicillin-streptomycin. The nanofibers and ECM controls were then transferred to the wells of a 24-well polystyrene plate pre-coated with 5% (m/v) Pluronic® F-127 (Sigma-Aldrich, Saint Louis, MO) to prevent cell attachment to the polystyrene. Cryopreserved PHHs (donor lots HUM4192, 16 year old Asian female, and HUM4055C, 54 year old Caucasian female) from Lonza (Walkersville, MD) were thawed, their viability was assessed using the Trypan Blue dye exclusion method, and then PHHs were seeded onto the above substrates at 200,000 cells in 500 µL per well of seeding medium containing phenol red-free high glucose DMEM with 10% fetal bovine serum (R&D Systems, Minneapolis, MN), 1.5% (v/v) N-2-hydroxyethylpiperazine-N'-2-ethanesulfonic acid (HEPES, Corning) buffer, 1% (v/v) insulin-transferrin-selenium-linoleic acid (ITS+) premix (Corning), 1% penicillin/streptomycin, 100 nM dexamethasone (Sigma-Aldrich), and 7 ng/mL glucagon (Sigma-Aldrich). The cultures were washed the next day once with phenol red-free DMEM once to remove unattached cells and the culture medium

was replaced with maintenance medium (similar recipe as seeding medium above but with 10% bovine calf serum). To create co-cultures, 100,000 3T3-J2s or LSECs in 500 µL per well were seeded onto PHH-laden nanofibers. For PHH-LSEC co-cultures, 20 ng/mL of human recombinant vascular endothelial growth factor (VEGF)-165 protein (Invitrogen, Waltham, MA) was added to the maintenance medium to maintain endothelial cell viability. The medium was replaced on all cultures every 2 days.

2.5. Cell viability and functional assessments

PrestoBlue™ (ThermoFisher, Waltham, MA) was used to assess cell viability/health according to manufacturer's protocol. Albumin in supernatants was measured using a sandwich-based enzyme linked immunosorbent assay (ELISA, Bethyl Laboratories, Montgomery, TX) with horseradish peroxidase detection and 3,3'5,5'-tetramethylbenzidine substrate (TMB, Rockland Immunochemicals, Boyertown, PA). Urea in supernatants was measured using diacetyl monoxime with acid and heat (Stanbio Labs, Boerne, TX) [31]. Absorbance of the samples was read on the Synergy H1 multimode plate reader (Biotech, Winooski, VT).

Cytochrome P450 (CYP) 3A4 and 2C9 enzyme activities were measured by incubating the cultures for 3 hours with luciferin-IPA (Promega Life Sciences, Madison, WI) or luciferin-H

(Promega), respectively, followed by the processing of collected supernatants per manufacturer's recommendations; luminescence was quantified with the Synergy H1 multimode reader. CYP1A2 and CYP2A6 enzymatic activities were measured by incubating the cultures for 3 hours with 5 μM 7-ethoxyresorufin (Sigma-Aldrich) or 50 μM coumarin (Sigma-Aldrich), respectively. The CYP2A6-generated metabolite, 7-hydroxycoumarin (7-HC), and CYP1A2-generated metabolite, resorufin, were quantified using fluorescence measurements (excitation/emission 355/460 nm for 7-HC and 550/585 nm for resorufin) on the Synergy H1 multimode reader.

2.6. Microscopy for cell visualization

Cultures were fixed with 4% (v/v) paraformaldehyde (PFA, Alfa Aesar, Wand Hill, MA) in ddH_2O for 20 minutes, rinsed three times with 1× PBS, and then incubated for 45 minutes at RT with a blocking solution containing 5% (v/v) donkey serum (Southern Biotech, Birmingham, AL) and 0.3% (v/v) Triton X-100 (Ameresco, Solon, OH) in 1× PBS. Goat anti-human albumin (Abcam, Cambridge, MA), rabbit anti-human cytokeratin 8 (CK8, Invitrogen), rabbit anti-human asialoglycoprotein receptor 1 (ASGR1, Proteintech, Rosemont, IL), mouse anti-human multidrug resistance-associated protein 2 (MRP2, Santa Cruz, Dallas, TX), mouse anti-human CD31 (Cell Signaling Technology, Danvers, MA), and mouse anti-human alpha-smooth

muscle actin (αSMA) (R&D Systems) primary antibodies were diluted at 1:200 in dilution solution containing 0.1% (m/v) bovine serum albumin (Sigma-Aldrich) and 0.3% Triton X-100 in 1× PBS and incubated on the cultures at 4°C overnight. Cultures were rinsed the next day with 1× PBS three times and then incubated with 1:100 diluted secondary antibodies, donkey anti-goat (Alexa Fluor 488, green), donkey anti-mouse (Alexa Fluor 647, Cy5) (Invitrogen), and donkey anti-rabbit (Alexa Fluor 568, red) for 1 hour at RT. DAPI (4',6-diamidino-2-phenylindole, MP Biomedicals, Solon, OH) at 300 nM concentration was added to the cultures for the last 15 minutes of the incubation period. After incubation, the cultures were rinsed with 1× PBS three times and observed under confocal microscopy with the filters of 638-755 nm for Cy5 and 410-488 nm for Alexa Fluor 488 and DAPI (Zeiss LSM 710, Zeiss, Germany; Olympus/Evident Scientific FV3000, Singapore). Maximum intensity images were obtained using ZEISS ZEN microscope software (Zeiss, Germany) and ImageJ.

For SEM, cultures were fixed for 45 minutes at RT with 3% (v/v) glutaraldehyde in ddH_2O containing 0.1 M sucrose and 0.1 M sodium cacodylate (Sigma-Aldrich), followed by incubation for 10 minutes in a solution containing 0.1 M sodium cacodylate and 0.1 M sucrose. The samples were then dehydrated by adding increased concentrations of ethanol (35, 50, 70, 100%, respectively) for 10 minutes each. Lastly, the samples were sputter coated with gold (15 nm) and imaged using the JSM-6500F JEOL SEM at an accelerating voltage of 15 kV.

2.7. Data analysis

Experiments were repeated 2 to 3 times with two PHH donors. Data analysis and visualization were performed using Microsoft Excel and GraphPad Prism (La Jolla, CA). Error bars represent standard deviation (2-3 technical replicates from a representative experiment). Statistical significance was determined via 2-way analysis of variance (ANOVA) with Tukey's or Dunnett's multiple comparisons tests.

3. Results

3.1. Morphological and mechanical characterization of the ECM fibers

We were able to successfully electrospin nanofibers composed of collagen (type I), PLECM, and their blends with chitosan. Uncrosslinked nanofibers displayed high porosity, a random orientation, and no beads were detected, though uncrosslinked nanofibers contained small particles in their structure, potentially due to the presence of insoluble fatty acids (**Figure 2A**). Average porosities of uncrosslinked nanofibers ranged from ~46% (collagen/PLECM) to ~58% (PLECM/chitosan), but were statistically similar (**Supplemental Table 3**). Average pore areas of uncrosslinked nanofibers ranged from ~0.3 μm^2 (collagen/chitosan and PLECM/chitosan)

to ~0.6 μm^2 (collagen/PLECM) with the exception being PLECM that displayed an average pore area of ~2.3 μm^2; however, pore areas for all nanofibers were statistically similar given the variations observed (**Supplemental Table 3**).

Following crosslinking, ECM nanofibers maintained their morphology (**Figure 2B**) and average porosities (~46% to 60%) but the average pore areas were generally lower for the crosslinked nanofibers (~0.15 to ~0.6 μm^2) as compared to the non-crosslinked nanofibers (~0.3 to ~2.3 μm^2) (**Supplemental Table 3**) due to swelling of the nanofibers after crosslinking. Following crosslinking, nanofibers containing chitosan showed agglomerates of fibers like beads (**Figure 2B**). Interestingly, the above-mentioned small particles present in the uncrosslinked collagen nanofibers appeared to have been removed following the washes of the crosslinking process. Chitosan-only nanofibers were crosslinked by glutaraldehyde vapor to avoid high swelling and loss of nanofiber morphology, which occurred in the 90% ethanol solution with EDC/NHS that was used to crosslink nanofibers containing collagen and/or PLECM. Furthermore, the ECM nanofibers displayed statistically similar nanoscale diameters before and after crosslinking (**Supplemental Table 2**). Lastly, chitosan-only nanofibers retained their morphology, diameters, and porosity following crosslinking, while 5% (w/v) PLECM-only solutions generated microfibers instead of nanofibers (**Supplemental Figure 2**).

The average Young's moduli for the fibers ranged from ~0.1 MPa (collagen/PLECM) to ~1.4 MPa (chitosan) (**Supplemental Table 4**). Along with collagen/PLECM nanofibers, the other nanofibers with lower average Young's moduli included PLECM (~0.3 MPa), collagen/chitosan (~0.3 MPa), and PLECM/chitosan (~0.4 MPa); in contrast, collagen nanofibers (~0.8 MPa), chitosan nanofibers (~1.4 MPa), and PLECM microfibers (~1.1 MPa) displayed higher average Young's moduli. Analogously, the maximum tensile stress was lowest for the softer nanofibers (collagen/PLECM ~0.2 MPa, PLECM ~0.8 MPa, collagen/chitosan ~1 MPa, and PLECM/chitosan ~1.2 MPa) and higher for the stiffer fibers (collagen nanofibers ~2.4 MPa, chitosan nanofibers ~5 MPa, and PLECM microfibers ~1.6 MPa). Lastly, the elongation at break of the fibers (i.e., tensile strain) were similar (~17% to 25%) except for PLECM-only nanofibers and microfibers, which had the lowest percentage strain of ~11% to 13% (**Supplemental Table 4**).

3.2. Biochemical characterization of the ECM fibers

XPS survey spectra for the ECM nanofibers and the individual constituent macromolecules showed peaks from carbon (C1s), oxygen (O1s), and nitrogen (N1s) but at different ratios (**Supplementary Figure 3A-B**). High-resolution XPS C1s spectra from all nanofibers showed peaks at ~287.5 eV, 285.5 eV, and 284 eV related to O=N-C and COOH groups, C-(O, N)

groups, and C-(C, H) groups, respectively, with some shifting on the binding energy (eV) and differences on the area/intensity of the peaks (**Figure 3B** and **Supplemental Figure 3E**). The relative intensity of the C-N groups compared to aliphatic carbon was higher in PLECM, likely due to a different protein composition than collagen alone (**Figure 3A**). Overall, the XPS data confirm that the macromolecules were incorporated into their respective nanofibers.

The FTIR spectra of the nanofibers containing collagen and/or PLECM showed similar peaks, likely because collagens are the majority components within PLECM. Characteristic absorptions were observed at ~3300 cm^{-1} (N-H stretching, amide A), ~3060 cm^{-1} (C-H stretching, amide B), ~1650 cm^{-1} (C=O stretching, amide I), ~1530 cm^{-1} (N-H deformation, amide II), and ~1280 cm^{-1} (coupled C-N stretching and N-H bending, amide III) (**Figure 3D**) [32-34]. Interestingly, the amide III peak at ~1280 cm^{-1} could only be observed in the collagen nanofiber spectra but not in the PLECM nanofiber spectra, whereas a peak at ~1200 cm^{-1} (C-N stretching) could only be observed on the PLECM but not on the collagen nanofiber spectra (**Supplementary Figure 3B**), suggesting that there are some structural differences across the two ECM types. Lastly, all features of the FTIR spectra of the nanofibers (**Figure 3D**) were present in the FTIR spectra of the corresponding individual macromolecules (**Figure 3C**).

3.3. Effects of ECM nanofibers on the morphology and secretory functions of PHH monocultures

PHHs maintained similar morphology for 23 days on nanofibers containing collagen and PLECM and adsorbed ECM control substrates as assessed via SEM, albeit fewer PHHs were observed on the adsorbed ECM controls, which is expected due to the typical loss of PHH viability/numbers on conventional (adsorbed ECM) stiff substrates [7]. Furthermore, PHHs appeared to have infiltrated into the nanofiber layers while maintaining their contacts with other neighboring cells (**Figure 4A**), whereas chitosan-only nanofibers resulted in lower PHH attachment and no apparent infiltration of PHHs into the nanofiber layers (**Supplemental Figure 4**).

Co-immunostaining for human albumin and human CK8 showed mostly single, sparsely distributed, and spread-out PHHs on the adsorbed ECM controls; in contrast, a larger number of PHHs were observed on the nanofibers, albeit PHH spreading patterns varied across the nanofibers, with PLECM and collagen/PLECM nanofibers containing less spread-out PHHs (**Figure 4B**), which is likely due to the lower Young's moduli of the PLECM (~0.3 MPa) and collagen/PLECM (~0.1 MPa) nanofibers allowing the PHHs to remain more spheroidal due to fewer traction forces as also seen on other soft substrates like gels composed of Matrigel [7].

Interestingly, while some PHHs displayed both albumin and CK8 staining, many spread-out PHHs only had detectable CK8 staining (**Figure 4B** and **Supplemental Figure 5**) suggesting loss of specialized liver functions (i.e., de-differentiation). Lastly, we also detected ASGR1 (hepato-specific marker) on PHHs cultured on nanofibers and adsorbed controls; while there were more ASGR1 positive PHHs on the nanofibers than the adsorbed controls, the expression of ASGR1 varied considerably across individual PHHs (**Supplemental Figure 6**), which may be due to variability in the extent/number of homotypic interactions in the local microenvironment of the cells.

PHH overall viability/health was similar over time across ECM nanofibers and adsorbed ECM controls, albeit values decreased by 20 to 40% after the first day of culture (**Figure 5C**), likely due to some cell detachment over the first week of culture as is common with other PHH monoculture models.

PHHs cultured on the adsorbed ECM controls secreted low but relatively stable levels of albumin (a widely utilized surrogate marker of liver protein synthesis) over 23 days, whereas albumin secretion rates on the ECM nanofibers increased over the first week of culture, remained relatively stable for 19 days, and then declined 7 to 30% by day 23 of culture; furthermore, the maximal albumin secretion rates were 4.2-fold higher on the collagen

nanofibers, 1.3-fold higher on the collagen/chitosan nanofibers, 5.4-fold higher on the collagen/PLECM nanofibers, 4.6-fold higher on the PLECM nanofibers, and 3.5-fold higher on the PLECM/chitosan nanofibers as compared to the adsorbed ECM controls (**Figure 5A**). Higher albumin secretion rates have been correlated with a higher differentiation status of PHHs [7], suggesting that the nanofibers better maintain PHH differentiated phenotype than adsorbed (conventional) ECM substrates.

In contrast to albumin secretion, PHH urea synthesis (a widely utilized marker of liver ammonia detoxification) rates displayed a continuous decline over time in all cultures (nanofibers and adsorbed ECM control substrates) and after 23 days had decreased by 90-98% from day 1 levels; however, urea synthesis rates were still 2.5-fold higher on the collagen nanofibers, 1.03-fold higher on the collagen/chitosan nanofibers, 1.8-fold higher on the collagen/PLECM nanofibers, 5.3-fold higher on the PLECM nanofibers, and 1.7-fold higher on the PLECM/chitosan nanofibers as compared to the adsorbed ECM controls after 23 days of culture (**Figure 5B**). Urea synthesis involves the coordinated action of several enzymes of the urea cycle and is typically difficult to maintain at steady levels in PHH monocultures even with various ECM combinations/manipulations [10]; therefore, it was not surprising here that nanofibers upregulated but did not stabilize urea synthesis in PHH monocultures as compared to adsorbed ECM substrates.

3.4. Effects of ECM nanofibers on the CYP enzyme activities of PHH monocultures

CYP enzymes are involved in the metabolism/biotransformation of most xenobiotics including 70–80% of all drugs in clinical use; the highest expressed forms in liver are CYPs 3A4, 2C9, 2C8, 2E1, and 1A2, while 2A6, 2D6, 2B6, 2C19 and 3A5 are less abundant [35]. Therefore, we measured the activities of less abundant (CYP2A6) and more abundant (CYPA2, 2C9, 3A4) CYP enzymes in PHHs on nanofibers and adsorbed ECM controls using well established fluorescent/luminescent high-throughput assays.

Maximal PHH CYP1A2 activities were 2.8-fold higher on the collagen nanofibers, 2.7-fold higher on the collagen/chitosan nanofibers, 3.1-fold higher on the collagen/PLECM nanofibers, 2.9-fold higher on the PLECM nanofibers, and 2.4-fold higher on the PLECM/chitosan nanofibers as compared to the adsorbed ECM controls (**Figure 5D**). Furthermore, while PHH CYP1A2 activity slowly declined over time in adsorbed ECM controls (30 to 35% of day 9 levels after 23 days), CYP1A2 activity on the nanofibers increased ~1.4- to 2.4-fold between 9 and 17 days and then declined ~60-80% between days 17 and 23 of culture (**Figure 5D**).

Maximal PHH CYP2A6 activities were 6-fold higher on the collagen nanofibers, 3.2-fold higher on the collagen/chitosan nanofibers, 6.6-fold higher on the collagen/PLECM nanofibers, 8.7-

fold higher on the PLECM nanofibers, and 3.6-fold higher on the PLECM/chitosan nanofibers as compared to the adsorbed ECM controls (**Figure 5E**). Furthermore, PHHs on the collagen/PLECM and PLECM/chitosan nanofibers displayed the highest CYP2A6 activity after 7 days; PHHs on the collagen nanofibers displayed the highest CYP2A6 activity after 15 days; PHHs on the collagen/chitosan and PLECM nanofibers displayed the highest CYP2A6 activity after 21 days (**Figure 5E**).

Maximal PHH CYP2C9 activities were 3.4-fold higher on the collagen nanofibers, 3.5-fold higher on the collagen/PLECM nanofibers, 2.4-fold higher on the PLECM nanofibers, and 3.2-fold higher on the PLECM/chitosan nanofibers as compared to the adsorbed ECM controls; in contrast, while maximal PHH CYP2C9 activity on the collagen/chitosan nanofibers (day 9) was ~7% lower than the adsorbed ECM controls, it was 1.5- to 2.5-fold higher between 17 and 23 days of culture (**Figure 5F**). Furthermore, while PHH CYP2C9 activities declined between 38% and 80% across all the cultures between 9 and 17 days of culture, CYP2C9 activities after 23 days of culture were still 2.7-fold higher on the collagen nanofibers, 1.5-fold higher on the collagen/chitosan nanofibers, 2.3-fold higher on the collagen/PLECM nanofibers, 3.5-fold higher on the PLECM nanofibers, and 1.4-fold higher on the PLECM/chitosan nanofibers as compared to the adsorbed ECM controls (**Figure 5F**).

Maximal PHH CYP3A4 activities were 3.6-fold higher on the collagen nanofibers, 1.1-fold higher on the collagen/chitosan nanofibers, 4.4-fold higher on the collagen/PLECM nanofibers, 3.6-fold higher on the PLECM nanofibers, and 3.2-fold higher on the PLECM/chitosan nanofibers as compared to the adsorbed ECM controls (**Figure 5G**). Furthermore, CYP3A4 activities increased 3- to 5.5-fold between days 7 and 15 for all the cultures, but then declined ~12% to 36% by day 21 (**Figure 5G**).

The results above show that while nanofibers can upregulate the activities of several different CYP isoforms as compared to adsorbed ECM substrates, they are unable to stabilize CYP levels for several weeks, which suggests that ECM manipulations alone are necessary but not sufficient to maintain CYP activities in PHHs over prolonged culture; we and others have previously seen something similar with other substrates in which ECM was the only microenvironmental manipulation for PHH monocultures in vitro [3, 7, 10].

3.5. Effects of PLECM microfibers on the phenotype of PHH monocultures

As on the nanofibers, PHHs on the 5% PLECM-only microfibers a) attached and infiltrated (**Supplemental Figure 4**), b) displayed similar viability over time as the adsorbed ECM controls (**Supplemental Figure 7A**), and c) displayed similar kinetics of albumin secretion

(**Supplemental Figure 7B**), urea synthesis (**Supplemental Figure 7C**), and CYP enzyme activities (**Supplemental Figure 7D-G**). Maximal albumin secretion on the PLECM-only microfibers was 4.3-fold higher, urea was 2.6-fold higher, CYP1A2 activity was 3-fold higher, CYP2A6 activity was 2.5-fold higher, CYP2C9 activity was 2.3-fold higher, and CYP3A4 activity was 3.2-fold higher than adsorbed ECM controls (**Supplemental Figure 7**). These results suggest that both nano- and microfibers allow for the upregulation of PHH functions as compared to adsorbed ECM substrates, likely due to the higher ECM surface area for PHHs to interact with on the fibrous matrices.

In contrast to PLECM-only microfibers, chitosan-only nanofibers caused a 60% reduction in the maximal PHH albumin secretion, a 73% reduction in CYP2C9 activity, and an 80% reduction in CYP3A4 activity as compared to the adsorbed ECM controls, while urea and CYP2A6 activity in chitosan-only nanofibers were undetectable after 3 weeks; however, maximal CYP1A2 activity on chitosan-only nanofibers was 3-fold higher than on the adsorbed ECM controls (**Supplemental Figure 7**). These results suggest that while the fibrous topography of the chitosan-only nanofibers can induce some PHH functions (e.g., CYP1A2) as compared to adsorbed ECM substrates, it is not sufficient to induce other PHH functions, likely due to lack of adequate adhesion sites and biochemical signaling afforded for by fibers generated using proteins present in the liver (i.e., collagen I and whole liver ECM).

3.6. Effects of ECM nanofibers on the morphology and secretory functions of co-cultures containing PHHs and 3T3-J2 fibroblasts

Since PHH monocultures displayed continuously declining urea synthesis and CYP2C9 activity even on the ECM nanofibers as discussed above, we established co-cultures of PHHs with 3T3-J2 fibroblasts, which were previously shown to improve the abovementioned functions on collagen-coated polystyrene [7], towards determining if ECM nanofibers could stabilize and further improve PHH functions in co-cultures over the adsorbed ECM controls. We executed co-cultures on adsorbed ECM (collagen or PLECM) controls and selected collagen, PLECM, collagen/PLECM, and PLECM/chitosan nanofibers for co-culture study, since they showed some of the highest functions for PHH monocultures as discussed above.

Upon co-cultivation with 3T3-J2 fibroblasts, PHHs maintained similar spheroidal morphology for 23 days on the nanofibers containing collagen and PLECM and adsorbed ECM control substrates as assessed via SEM, albeit fewer PHHs were observed on the adsorbed ECM controls; interactions between the two cell types on the nanofibers were observed in high magnification SEM images (**Figure 6A**). Co-immunostaining for human albumin and human CK8 showed that PHHs formed colonies around the mouse fibroblasts across all tested culture formats; however, in contrast to the adsorbed ECM controls, a greater number and larger PHH

colonies were observed on the nanofibers, especially collagen, PLECM, and collagen/PLECM nanofibers (**Figure 6B**). Additionally, PHHs displayed both albumin and CK8 staining on most of the nanofibers and particularly on the PLECM and collagen/PLECM nanofibers, (**Figure 6B** and **Supplemental Figure 8**). Lastly, we also detected ASGR1 and MRP-2 (major transporter present on the apical/canaliculi surface of hepatocytes) on PHHs cultured on nanofibers and adsorbed controls, albeit MRP2 staining patterns were dependent on PHH cluster size with larger clusters containing a greater number of MRP-positive bile canaliculi between adjacent PHHs; the fibroblasts were positive for α-SMA (**Supplemental Figure 9**). These results show that PHHs maintain several major differentiated phenotypic markers (albumin, CK8, ASGR1, MRP2) when co-cultured with the fibroblasts on the nanofibers, albeit the expression of these markers is dependent on the colony size, which is expected since local homotypic interactions between PHHs are known to influence their differentiated state [7].

Co-cultures on the adsorbed ECM controls displayed peak albumin secretion by day 15, which then declined by 11 to 32% between 15 and 23 days of culture. In contrast, albumin secretion on the nanofibers peaked by day 15 and remained relatively steady for 23 days (**Figure 7A**). Interestingly, co-cultures showed 2.2-fold higher albumin secretion on the adsorbed collagen control as compared to the adsorbed PLECM control. Furthermore, the maximal albumin secretion rates were 3.7-fold higher on the collagen nanofibers, 1.9-fold higher on the PLECM

nanofibers, 2.7-fold higher on the collagen/PLECM nanofibers, and 3.2-fold higher on the PLECM/chitosan nanofibers as compared to the adsorbed collagen control (**Figure 7A**).

Co-culture urea synthesis declined by 57 to 67% of day 3 levels after 9 days in culture on the adsorbed ECM controls, though co-cultures synthesized 2- to 3-fold higher urea on adsorbed collagen as compared to adsorbed PLECM. In contrast, co-cultures on the nanofibers showed either relatively stable (PLECM and collagen/PLECM) or increasing urea synthesis over time (PLECM/chitosan up to 1.9-fold and collagen up to 1.3-fold relative to day 3 levels) (**Figure 7B**). Furthermore, the urea synthesis rates were 5.9-fold higher on the collagen nanofibers, 3-fold higher on the PLECM nanofibers, 3.7-fold higher on the collagen/PLECM nanofibers, and 6-fold higher on the PLECM/chitosan nanofibers as compared to the adsorbed collagen control after 23 days (**Figure 7B**).

The results above show that in contrast to PHH monocultures, co-culture with fibroblasts upregulates and stabilizes *both* PHH albumin and urea secretions, suggesting that the synergy between the nanofiber composition/topography and signaling from the fibroblasts is important for such outcomes than possible on adsorbed ECM substrates.

3.7. Effects of ECM nanofibers on the CYP enzyme activities of co-cultures containing PHHs and 3T3-J2 fibroblasts

CYP1A2 activities in all the co-cultures decreased between 9 and 17 days and then increased by day 23 to levels higher than levels on day 9; furthermore, maximal co-culture CYP1A2 activities were 1.4-fold higher on the collagen nanofibers, 1.7-fold higher on the PLECM nanofibers, 1.5-fold higher on the collagen/PLECM nanofibers, and 1.6-fold higher on the PLECM/chitosan nanofibers as compared to the adsorbed collagen control (**Figure 7C**).

In contrast to CYP1A2, CYP2A6 activities in all the co-cultures increased over time; additionally, maximal co-culture CYP2A6 activities were 8.4-fold higher on the collagen nanofibers, 4.4-fold higher on the PLECM nanofibers, 4.7-fold higher on the collagen/PLECM nanofibers, and 12.5-fold higher on the PLECM/chitosan nanofibers as compared to the adsorbed collagen control, which itself had 2-fold higher maximal CYP2A6 activity than the adsorbed PLECM control (**Figure 7D**).

As with CYP2A6, CYP2C9 activities in all co-cultures increased over time; additionally, maximal co-culture CYP2C9 activities were 3.2-fold higher on the collagen nanofibers, 1.7-fold higher on the PLECM nanofibers, 2.1-fold higher on the collagen/PLECM nanofibers, and

4.6-fold higher on the PLECM/chitosan nanofibers as compared to the adsorbed collagen control, which itself had 6.5-fold higher maximal CYP2C9 activity than the adsorbed PLECM control (**Figure 7E**).

Lastly, CYP3A4 activities peaked after 15 days across all the co-cultures except the PLECM/chitosan nanofibers that displayed highest activity after 7 days, and then declined between 27 and 52% from the peak activity by 21 days; furthermore, maximal co-culture CYP3A4 activities were 2.5-fold higher on the collagen nanofibers, 1.1-fold higher on the PLECM nanofibers, 2.6-fold higher on the collagen/PLECM nanofibers, and 1.6-fold higher on the PLECM/chitosan nanofibers as compared to the adsorbed collagen control, which itself had 1.4-fold higher maximal CYP3A4 activity than the adsorbed PLECM control (**Figure 7F**).

The results above show that while the synergy between nanofiber composition/topography and fibroblast co-culture can upregulate both abundant (CYP1A2, 2C9, 3A4) and less abundant (CYP2A6) CYPs over prolonged culture as compared to adsorbed ECM substrates, such a synergy is able to better stabilize some CYP isoforms (CYP2A6, 2C9) than others (CYP1A2, 3A4) over ~3 weeks of culture.

3.8. Long-term functions of PHH/3T3-J2 co-cultures on the collagen/PLECM nanofibers

Next, PHH/3T3-J2 were co-cultured for 47 days on the collagen/PLECM nanofibers that showed the highest CYP3A4 activity above, while using adsorbed collagen as a control. Even after 47 days, we detected PHHs and 3T3-J2s via SEM and immunostaining on the above substrates (**Supplemental Figure 10**). At the functional level, once co-cultures on the nanofibers reached their peak albumin secretion rates over 15 to 19 days, the levels remained relatively stable for 35 days in culture, after which a decline was observed down to 27% of the peak levels by day 47; nonetheless, even after 47 days, albumin secretion rates in co-cultures on the nanofibers were 3.6-fold higher than the adsorbed collagen control (**Supplemental Figure 11A**). Urea synthesis had similar trends as albumin above, with a 5-fold higher rate observed as compared to the adsorbed collagen control even after 47 days in culture (**Supplemental Figure 11B**). CYP1A2 activity was relatively stable in the co-cultures for 45 days, while CYP2A6, 3A4, and 2C9 activities peaked by 3 weeks and then displayed variable decline rates over 47 days; however, even after 47 days, CYP2A6 was 5-fold higher, CYP3A4 was 34-fold higher, and CYP2C9 was 17-fold higher on the collagen/PLECM nanofibers as compared to the adsorbed collagen control (**Supplemental Figure 11C-F**). The results above show that while the synergy between nanofiber composition/topography and fibroblast co-culture can upregulate several major functions of the liver for ~7 weeks of culture as compared

to adsorbed ECM controls, the optimal window of functional stability (for drug screening and other biological inquiries) is ~3 weeks.

3.9. Effects of ECM nanofibers on the phenotype of co-cultures containing PHHs and human LSECs

Since the 3T3-J2 fibroblasts are of mouse origin, their co-culture with PHHs is useful for drug screening applications as we and others have shown previously [1], but not for applications in regenerative medicine (i.e., cell-based therapy). In contrast, LSECs are present in the liver and previous studies with rat hepatocytes have shown that these cells can stabilize some hepatic functions on adsorbed ECM substrates [36]. However, we have shown that *human* LSECs are unable to stabilize PHH functions on adsorbed ECM substrates without the inclusion of the 3T3-J2 fibroblasts [37].

Here, we hypothesized that the synergy between nanofiber composition/topography and LSEC interactions could mitigate the above limitation with PHH/LSEC co-cultures on adsorbed ECM substrates. Towards that end, we generated PHH/LSEC co-cultures on the same nanofibers and adsorbed ECM control substrates as those used for PHH/3T3-J2 co-cultures above. Immunostaining for CD31 and albumin showed the presence of endothelial cells and

PHHs across all culture formats, respectively, albeit significantly fewer endothelial cells and PHHs were observed on the PLECM adsorbed control (**Supplemental Figure 12**), which was unexpected given the physiological relevance of PLECM over collagen-I alone. Co-immunostaining for albumin and CK8 showed that many spread-out PHHs had detectable CK8 but not albumin, and PHHs on collagen nanofibers were less spread-out but fewer in numbers than the other conditions (**Supplemental Figure 12**), which suggests that some PHHs de-differentiate in the PHH/LSEC co-cultures irrespective of substrate type.

PHH/LSEC co-cultures on the adsorbed ECM controls displayed precipitously declining albumin and urea secretions (**Supplemental Figure 13A-B**), which is consistent with our previous findings on PHH/LSEC co-cultures fabricated on polystyrene with adsorbed collagen I [37]. In contrast, albumin secretion either remained relatively stable or increased over time in PHH/LSEC co-cultures on the selected ECM nanofibers, though maximal secretions in co-cultures on the nanofibers were 3.7- to 18.6-fold lower than the maximal secretions in corresponding PHH/3T3-J2 co-cultures (**Figure 7A**). However, urea synthesis in the PHH/LSEC co-cultures displayed the same precipitous decline across all the substrates as that observed with PHH monocultures above. Lastly, CYP activities in the PHH/LSEC co-cultures were generally statistically similar over time on the nanofibers as compared to adsorbed ECM controls (**Supplemental Figure 13C-F**).

The results above suggest that the major contributors to the upregulation and stabilization of albumin secretion are the nanofiber composition and topography as opposed to co-culture with LSECs since the functional rends on nanofibers versus adsorbed ECM substrates were similar across PHH monocultures and PHH/LSEC co-cultures, whereas they were significantly different (more differentiated over several weeks in vitro) in PHH/3T3-J2 co-cultures, potentially due to key liver-like molecules secreted/presented by the fibroblasts [38, 39].

4. Discussion

Previous studies have utilized synthetic polymers alone or those blended with a concentrated liver ECM solution to generate nanofibers for liver culture [40, 41]. In contrast, here we modified several steps of the decellularization process to prepare dry PLECM for electrospinning without the need for synthetic polymers, including pepsin-based digestion of PLECM to break crosslinked sites on ECM and subsequently removing pepsin via dialysis and lyophilizing. Our protocol should be applicable with few modifications to human LECM, though PLECM may still be most suited for human liver cell culture given the unpredictable conditions and quality of the transplant-rejected human livers [9].

Synthetic or hydrophobic macromolecules are typically used for generating nanofibers for cell

culture since they are stable in polar cell culture medium, easy to handle, and do not require chemical crosslinking [1, 29, 42-44]. However, tissue-derived ECM can better support the functions of rodent hepatocytes [13-15] and transformed hepatic cell lines [17, 18], and thus it is desirable to generate nanofibers from such ECM for PHH culture. Here, we overcame the difficulties associated with using hydrophilic ECM biomolecules by a) electrospinning directly onto glass coverslips to enable microscopic imaging of the cells via transmitted light microscopy and b) chemically crosslinking the nanofibers using EDC/NHS in 90% ethanol (glutaraldehyde vapor for chitosan-only due to swelling in ethanol) to allow for easier handling of the nanofibers in culture. PLECM at 2% (w/v) could be used in combinations with other ECM molecules to generate nanofibers but using PLECM at 5% (w/v) led to the formation of microfibers, the mechanisms of which are not clear but could be related to components within PLECM adhering more strongly to each other at higher concentrations during electrospinning; nonetheless, all nanofibers maintained statistically similar diameter ranges before and after crosslinking (~200 nm), which allowed us to test the effects of nanofiber composition on hepatic functions as opposed to wide variations in diameter.

Nanofibers fabricated using collagen I, PLECM, and their blends maintained fiber morphology and average porosities (~46% to ~60%) following crosslinking; however, the average pore areas decreased for some of the nanofibers following crosslinking, likely due to a high degree

of swelling in the 90% ethanol-containing crosslinking solution [45]. Nonetheless, cells were still able to interact with and penetrate into several of the crosslinked nanofibers. Furthermore, collagen/PLECM (~0.1 MPa Young's modulus), PLECM (~0.3 MPa), collagen/chitosan (~0.3 MPa), and PLECM/chitosan (~0.4 MPa) nanofibers were softer than the collagen-only and chitosan-only nanofibers (~0.8 to 1.4 MPa), potentially due to non-collagen molecules present in PLECM and chitosan interfering with the tight crosslinking/packing between collagen-I molecules. While the stiffness of the nanofibers is higher than that of native liver (~0.5kPa to 4 kPa) [46, 47], it is three orders of magnitude lower than plastic or glass (GPa). Lastly, comparison of the FTIR and XPS spectra of the fibers and the individual macromolecules showed similar polarizable functional groups and elemental compositions, respectively, suggesting that the electrospinning process did not significantly change the biochemistry of the ECM.

When incubated in cell culture medium, pure collagen, pure PLECM, and collagen/chitosan nanofibers lost some porosity and changed morphology over time as compared to the collagen/PLECM and PLECM/chitosan blended fibers that maintained porosity and morphology even after 23 days. It is possible that unlike pure collagen I, PLECM has other proteins (e.g., collagen IV) that act to provide mechanical stability to the collagen or chitosan fibrillar ECM scaffold [48], and the higher total concentrations of macromolecules in the

collagen/PLECM and chitosan/PLECM blends used for electrospinning generated additional sites for interaction and crosslinking than PLECM alone [25, 49, 50]. Regardless of the variable morphological stability of different nanofiber compositions in cell culture medium over several weeks, they were suitable for liver cell culture and phenotypic assessments.

SEM showed that PHHs maintained similar morphology for several weeks on nanofibers containing collagen and PLECM, whereas PHH numbers were considerably lower on the adsorbed ECM controls following prolonged culture. In contrast, chitosan-only nanofibers resulted in lower PHH attachment which may be due to the lack of collagens typically needed for robust PHH attachment. Immunostaining showed that PHHs on nanofibers were positive for intermediate filament, CK8; however, co-expression of more differentiated/specialized markers, albumin and ASGR1, was variable across PHHs on nanofibers, suggesting some level of PHH de-differentiation in monocultures even on nanofibers.

After a 20-40% drop in PHH viability over 7 days, values were relatively stable until 23 days; such a drop in viability is likely due to PHH death and detachment, as is common with other culture models [3], given that not all viable PHHs that attach to a substrate will survive *in vitro* due to the variable health of cells isolated from human livers. Despite this loss of some viability in the first week, nanofibers caused to up to ~5-fold higher maximal albumin secretion, ~3-fold

higher CYP1A2 activity, ~9-fold higher CYP2A6 activity, ~3.5-fold higher CYP2C9 activity, and ~4-fold higher CYP3A4 activity than adsorbed ECM. PLECM-only nanofibers caused the highest maximal CYP2C9 activity while collagen/PLECM nanofibers caused the highest maximal levels for other functions (albumin, urea, and CYP1A2/2A6/3A4 activities). Collagen-only nanofibers generally ranked second or third in the induction of maximal functions, while PLECM/chitosan and collagen/chitosan blended nanofibers ranked lowest in their induction of PHH functions. Even PLECM microfibers (~1 μm) caused similar induction of functions in PHH monocultures as nanofibers, which suggests that the ability of cells to interact with a larger surface area of fibers in the ~200-1000 nm range is beneficial for the induction of PHH functions over adsorbed ECM.

While others have shown the independent effects of ECM stiffness [46, 51, 52] and porosity [53] on hepatocyte functions, our study is the first to evaluate the synergistic effects of ECM stiffness, topography, porosity, and available surface area for cell attachment/infiltration on the long-term functions of PHHs. The nanofibers were found to be significantly softer (~0.1 to 1.4 MPa) than glass/plastic and lower stiffness (protein hydrogels) has been previously shown to maintain differentiated functions of mouse hepatocytes via enhanced expression of master transcription factor, hepatocyte nuclear factor 4 alpha (HNF4alpha) [46]. HNF4alpha expression is inhibited by stiffer surfaces through the induction of the Rho/Rho-associated

protein kinase pathway; whether such a mechanism partly underlies the functional upregulation in PHHs on our nanofiber-based platform remains to be elucidated. Another variable that likely is important for the functional upregulation in PHHs on nanofibers is porosity since previously collagen foams with pore size between 10 and 80 μm caused 50-fold higher albumin secretion in hepatocytes than non-porous gels [53], presumably due to better transport of key signaling molecules throughout the culture in the porous constructs. However, neither porosity nor topography were sufficient to induce the highest or most stable PHH functions here as shown with chitosan-only nanofibers relative to the liver ECM-based nanofibers; such an outcome is not entirely unexpected since PHHs are adherent cell types that function better on collagenous substrates as opposed to substrates containing non-collagenous proteins [10], likely due to optimal focal adhesion formation and ensuing formation of a cortical actin network near the cell membranes (versus actin stress fiber formation) that helps stabilize bile canaliculi towards polarizing the hepatocyte [54]. Lastly, since PLECM-only and collagen/PLECM nanofibers induced the highest PHH functions than collagen-only and chitosan-blended collagen or PLECM nanofibers, we hypothesize that the optimal combinations and concentrations of liver ECM proteins (e.g., collagens III and IV, fibronectin, laminin) in PLECM were responsible for such outcomes whereas presence of chitosan inhibited PHH interactions with their native ECM proteins; indeed, in previous studies using recombinant liver inspired ECM proteins spotted onto microarray substrates, we have shown

that specific ECM combinations can unexpectedly either induce or inhibit PHH functions [10], likely via complex and yet undiscovered mechanotransduction mechanisms that target hepatic transcription factors such as HNF4alpha.

Urea and CYP2C9 activity showed a precipitous decline in PHH monocultures on nanofibers, which is consistent with previous findings that ECM manipulations alone are necessary but not sufficient to stabilize diverse hepatic functions [55, 56]. In contrast, 3T3-J2 fibroblasts were previously shown to induce and stabilize hepatic functions, including CYP2C9 activity and urea synthesis, for several weeks on adsorbed ECM, though levels need further enhancement to be closer to physiological levels [4, 7]. Thus, here we generated PHH/3T3-J2 co-cultures to determine if an *in vivo*-like fibrous ECM scaffold could further induce hepatic functions than the adsorbed ECM.

ECM nanofibers coupled with fibroblasts led to a 3D/spheroidal PHH morphology for 23 days. Most PHHs in the co-cultures co-expressed CK8, albumin, ASGR1, and MRP2, suggesting a well-differentiated and polarized phenotype. Additionally, PHH/fibroblast co-cultures on nanofibers showed up to 3.7-fold higher maximal albumin secretion, 6-fold higher urea synthesis, 1.7-fold higher CYP1A2 activity, 12.5-fold higher CYP2A6 activity, 4.6-fold higher CYP2C9 activity, and 2.6-fold higher CYP3A4 activity than on adsorbed ECM. Both albumin

and urea secretions in co-cultures on the nanofibers either increased or remained relatively stable once steady state was reached, whereas secretions declined in co-cultures on the adsorbed ECM, albeit not in the same precipitous way as with PHH monocultures. CYP2C9, 1A2, and 2A6 activities showed similar trends as albumin and urea secretions, whereas CYP3A4 activity showed a 27% decline from its peak value by day 23.

Functional assessment of PHH/3T3-J2 co-cultures on the collagen/PLECM nanofibers for 47 days showed that the relative stability of albumin/urea secretions and CYP activities was maintained for ~5 weeks and ~3 weeks, respectively, except for CYP1A2 activity that displayed stability for the full 47 days. Nonetheless, even after 47 days, albumin/urea secretions and CYP2A6 activity were 3.6- to 5-fold higher, while CYP3A4 and CYP2C9 activities were 17- to 34-fold higher in co-cultures on the nanofibers as compared to the adsorbed ECM. Lastly, the presence of the fibroblasts appeared to stabilize nanofiber morphology for long-term cultures, potentially due to additional ECM secreted by the fibroblasts to mechanically stabilize the fibrous scaffold.

We previously showed that the 3T3-J2 fibroblasts induce the highest level of functions in PHHs on adsorbed ECM relative to primary LSECs [37], Kupffer cells [57], and hepatic stellate cells [58], which may be due to the de-differentiation of these liver NPCs that also occurs alongside

that of PHHs *in vitro*. In contrast, the embryonic 3T3-J2 fibroblasts could potentially provide developmentally appropriate differentiation cues to prevent PHH de-differentiation *in vitro*; indeed, 3T3-J2 fibroblasts express molecules present in the liver, including truncated-cadherin [38] and decorin [39], though the multifactorial mechanism by which these fibroblasts induce the functions of hepatocytes from multiple species remains unelucidated. Nonetheless, here we hypothesized that on a more *in vivo*-like ECM substrate, LSECs could induce PHH functions to a higher degree than on adsorbed ECM and potentially at higher levels than the murine fibroblasts. We found that, in contrast to a precipitous decline on adsorbed ECM controls, albumin secretion remained relatively stable or increased over time in PHH/LSEC co-cultures on PLECM and/or collagen nanofibers, though levels were still lower than in the PHH/3T3-J2 co-cultures. Other measured functions (urea and CYP activities) were statistically similar across PHH/LSEC co-cultures on the nanofibers and adsorbed ECM, suggesting that LSEC-mediated support of PHHs may necessitate additional microenvironmental cues, such as further culture medium optimizations and/or co-culture with other liver NPCs, to be fully physiologically-relevant and optimal. Lastly, while we used passaged LSECs here to obtain sufficient numbers for co-culture with PHHs, freshly isolated human LSECs that better retain their in vivo-like phenotype (e.g., fenestrae) may induce higher levels of PHH functions, albeit such cells are logistically and economically difficult to implement for routine experimentation.

Even though of murine origin, 3T3-J2 fibroblasts have been previously shown extensively to not interfere with the use of stabilized PHHs in co-cultures for drug metabolism [59] and toxicity [60] screening and to model key features of global diseases, such as hepatitis B viral infection [61], malaria infection [62], and non-alcoholic fatty liver disease [63]. Thus, we anticipate that the functionally enhanced PHH/3T3-J2 co-cultures on ECM nanofibers can be utilized for similar *in vitro* applications, but with a more *in vivo*-like ECM scaffold and higher functions than on adsorbed ECM, while co-cultures containing only human and liver cells will be best suited for use in regenerative medicine.

In conclusion, we developed a novel protocol to electrospin PLECM and collagen I into nanofibers without the need for synthetic polymer blends. We then utilized these natural ECM nanofibers to show for the first time that PHH functions are significantly enhanced for several weeks on the ECM nanofibers relative to the conventionally adsorbed ECM controls, and that PHH/3T3-J2 co-cultures display higher and stable functions for 5 weeks on the nanofibers than on the adsorbed ECM controls. We anticipate that our platform can be utilized in the future for drug screening, disease modeling, and regenerative medicine, as well as to investigate the molecular mechanisms underlying the effects of ECM composition and topography on human liver functions.

Acknowledgments

The authors gratefully acknowledge the financial support from the National Science Foundation (Award Number 1933552 to S.R.K and M.J.K). We also would like to thank the Colorado State University Analytical Resources Core Facility (RRID: SCR_021758) and the Fluorescence Imaging Core (FIC) via the Research Resources Center (RRC) at the University of Illinois at Chicago.

Figures and Figure Legends

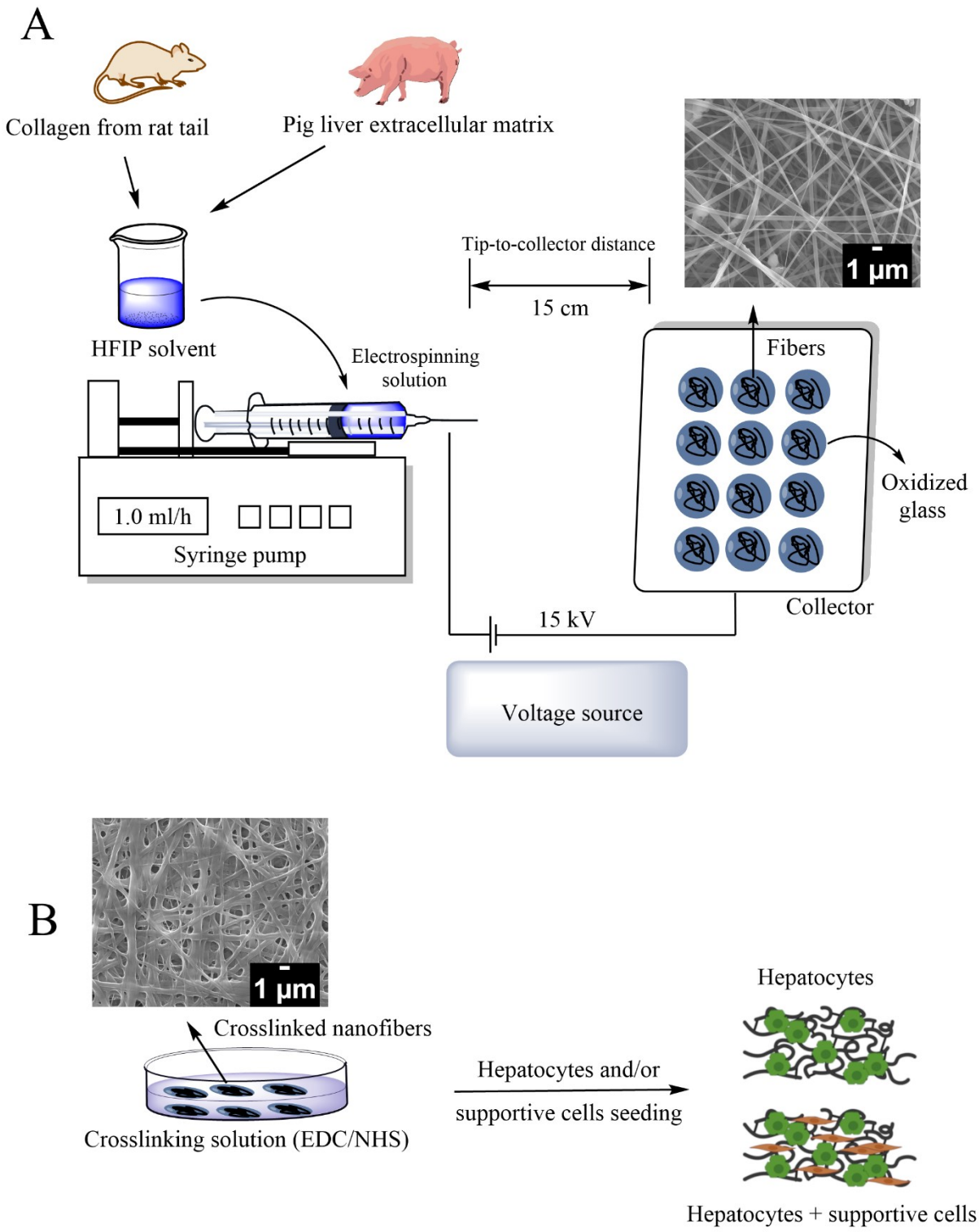

Figure 1: Scheme of the preparation of *in vitro* liver models. (A) Collagen extracted from rat tail and/or PLECM extracted from porcine liver were dissolved in HFIP and electrospun

over 6 to 8 hours varying the flow rate, voltage and distance from the needle to the collector. The fibers were collected on oxidized glass. (B) Crosslinked nanofibers were seeded with hepatocytes and/or supportive cells and cultured over several days. Created with ChemDraw and BioRender.com.

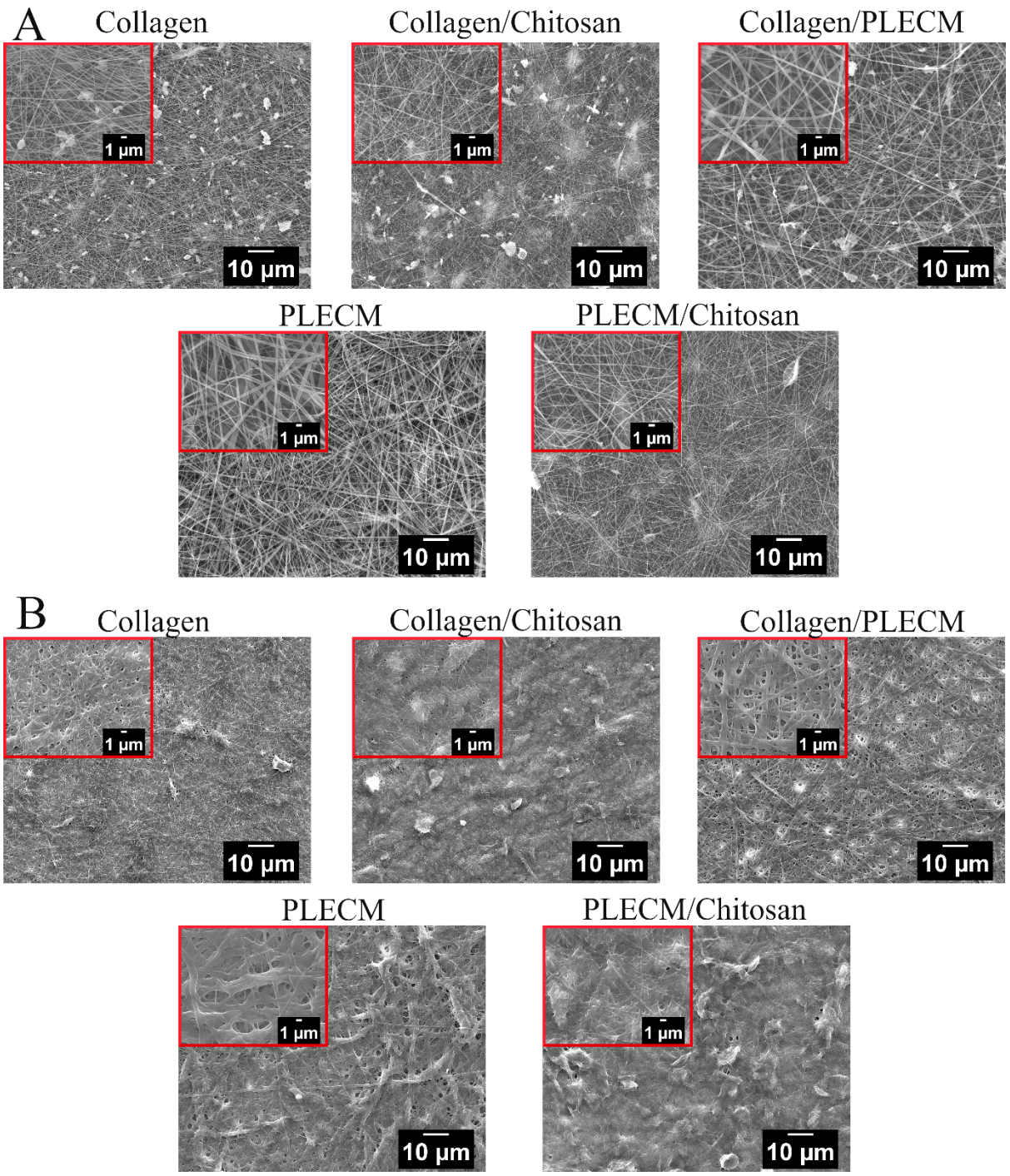

Figure 2: SEM images of nanofibers. (A) Uncrosslinked and (B) chemically crosslinked nanofibers.

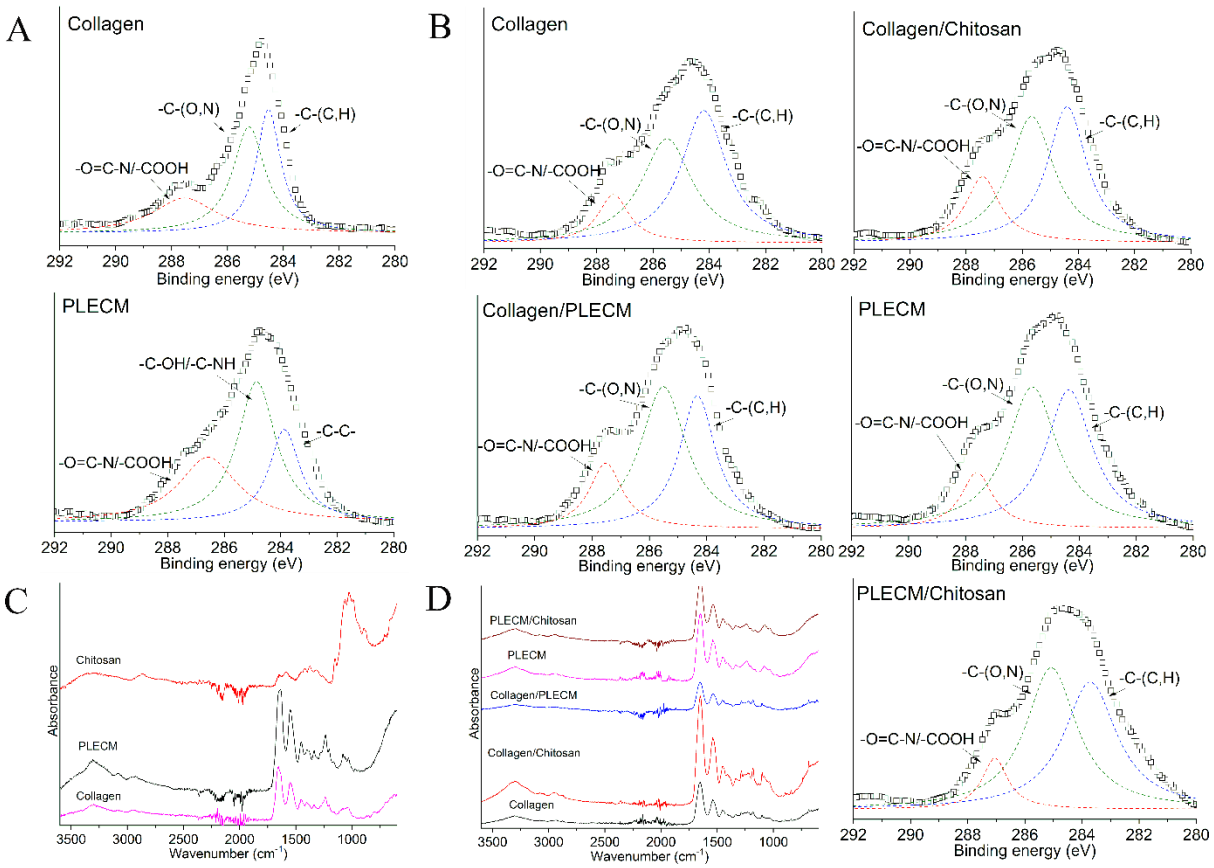

Figure 3: Physicochemical characterization of nanofibers. (A) C1s high-resolution XPS spectra of macromolecules, (B) C1s high-resolution XPS spectra of nanofibers, (C) FTIR of individual macromolecules, and (D) FTIR spectra of nanofibers.

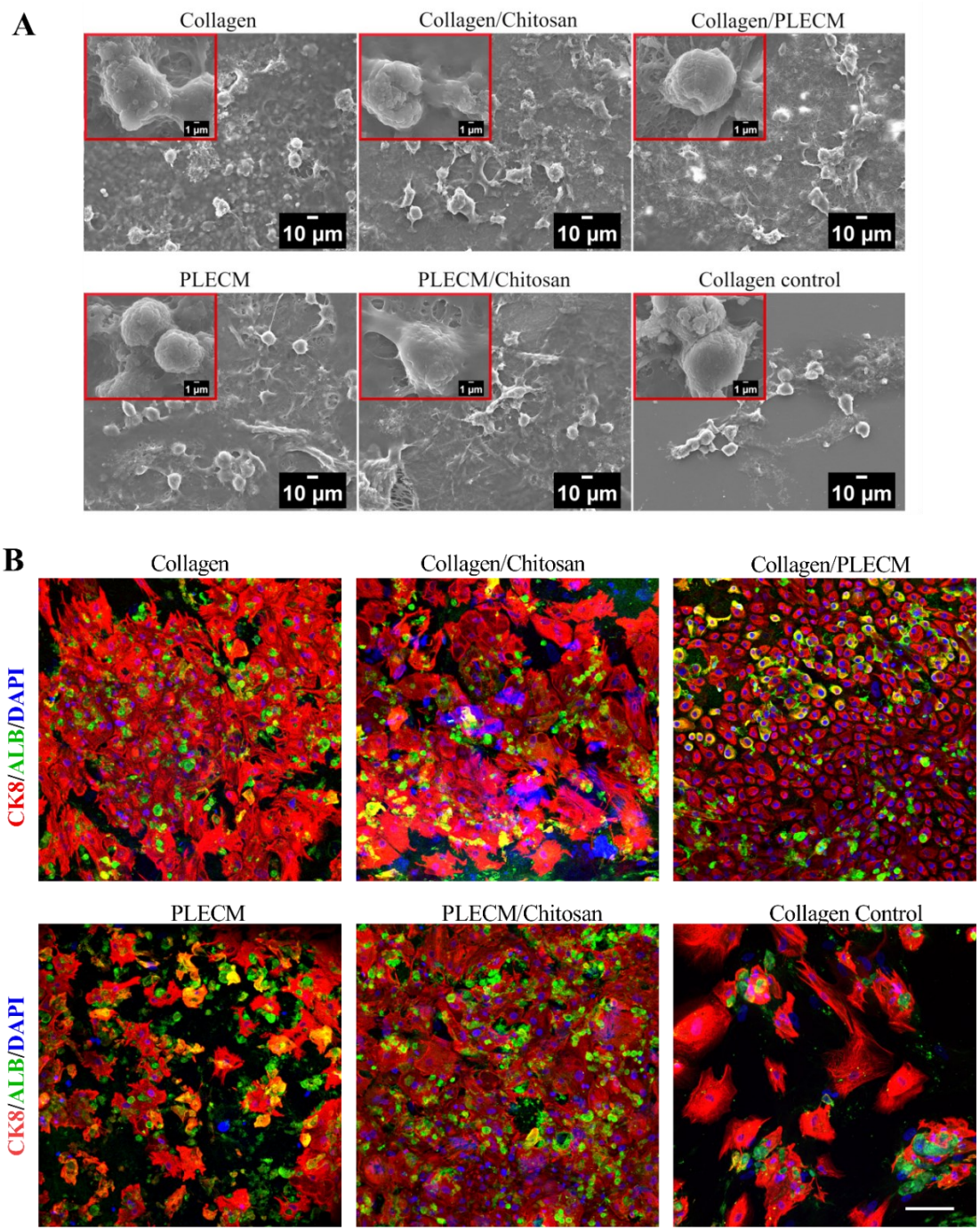

Figure 4: SEM and confocal microscopy images of PHH monocultures on ECM nanofibers and adsorbed collagen I control. (A) SEM and (B) confocal microscopy images after 23 days of culture. For immunostaining, cultures were fixed and stained for antibodies against human albumin (hepatocyte marker, green), CK8 (hepatocyte marker, red), and DAPI (nucleus, blue). Scale bar for panel B = 100 µm.

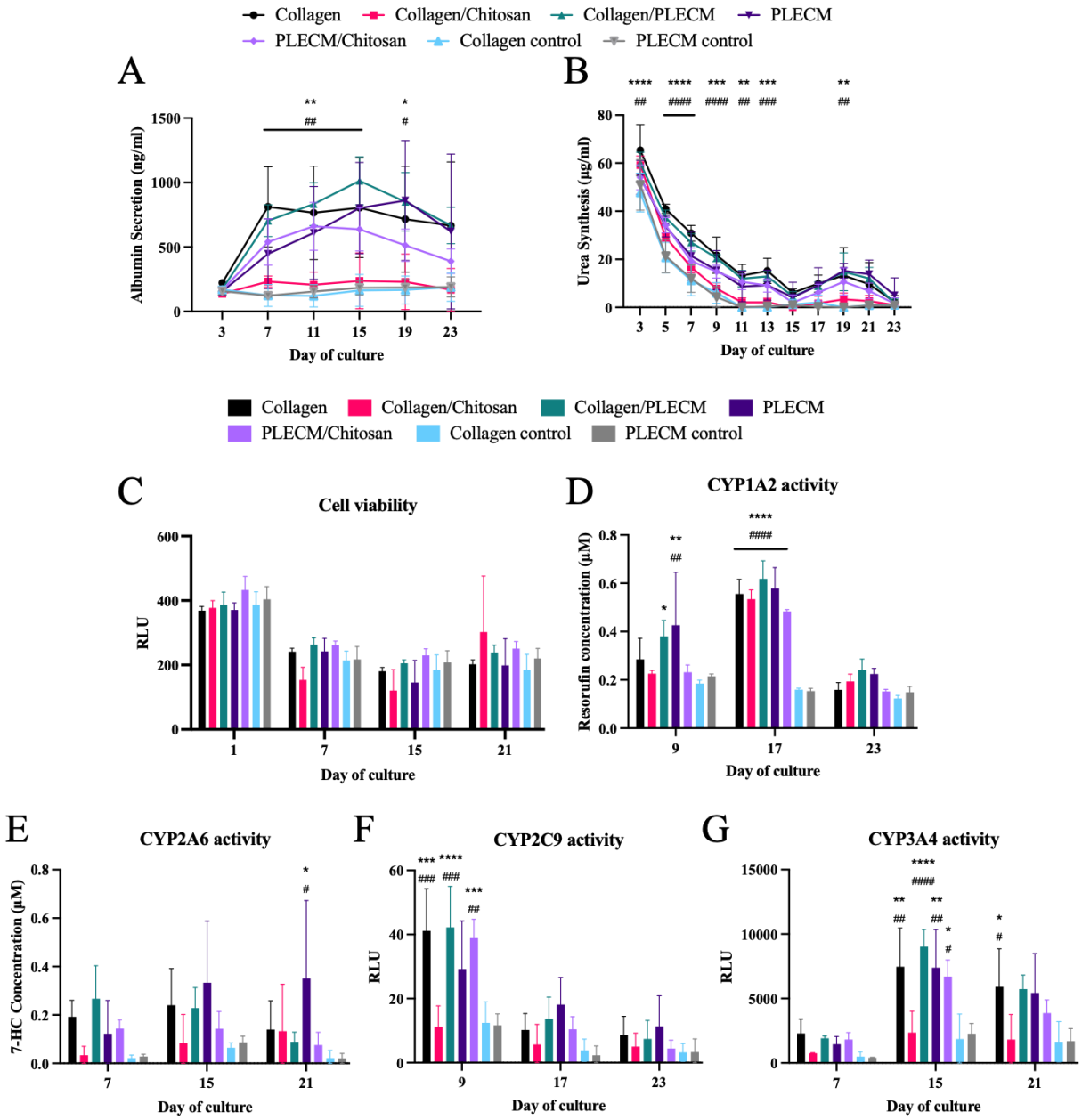

Figure 5: PHH monoculture viability and functions on nanofibers and adsorbed ECM controls. (A) Albumin secretion, (B) urea synthesis, (C) cell viability (PestoBlue), (D) CYP1A2, (E) CYP2A6, (F) CYP2C9, and (G) CYP3A4 enzymes activities of PHH monocultures on the nanofibers and adsorbed ECM controls. Asterisks (*) indicate statistical significance relative to the adsorbed collagen control and hash (#) indicates significance relative to the adsorbed PLECM control. * or # p<.05, ** or ## p<.01, *** or ### p<.001, **** or #### p<.0001. Panels

A and B show statistical comparisons for collagen-only nanofibers, while statistical comparisons for other nanofibers are shown in Supplemental Table 5.

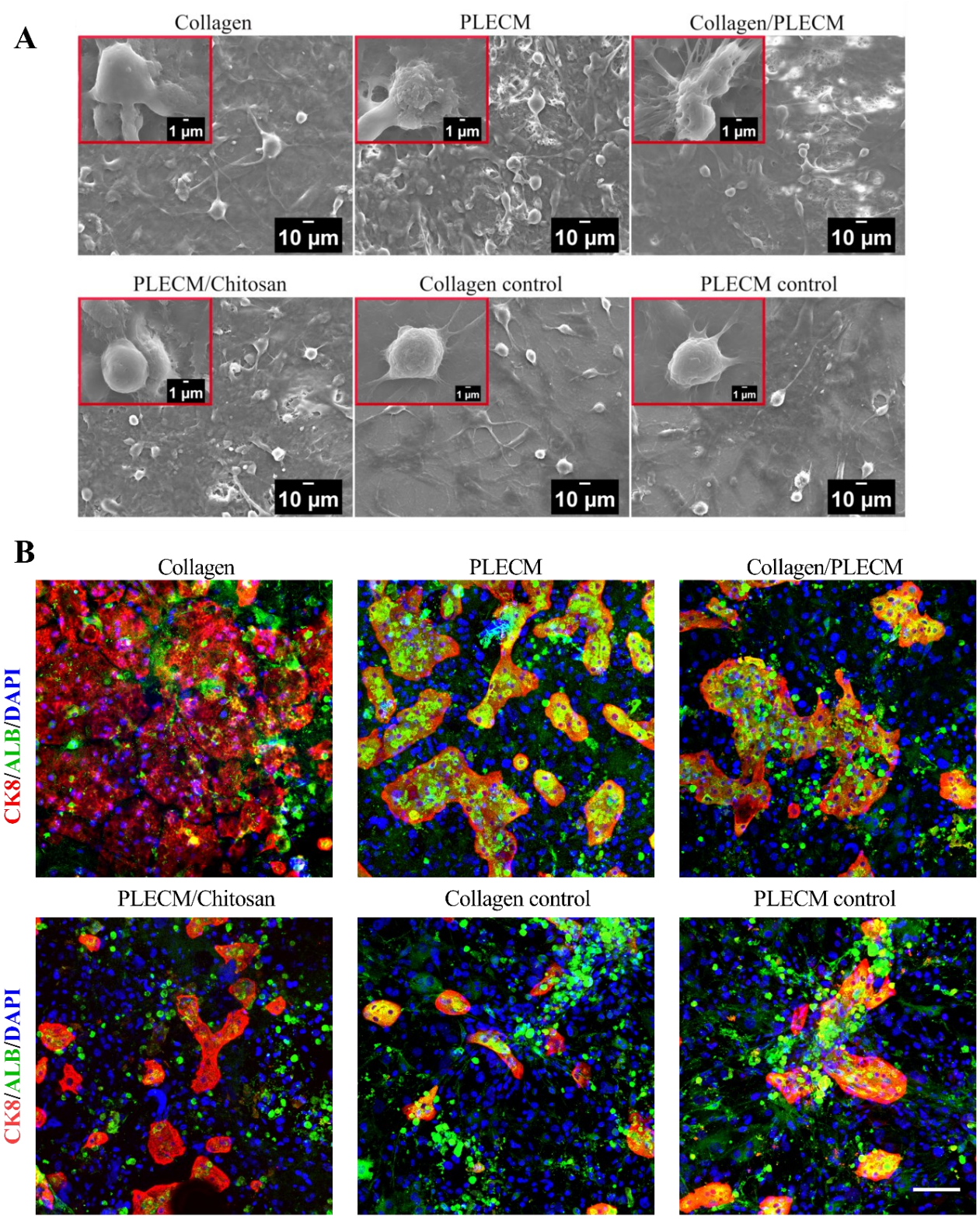

Figure 6: SEM and confocal microscopy images of PHH/3T3-J2 co-cultures on ECM nanofibers and adsorbed ECM control. (A) SEM and (B) confocal microscopy images after

23 days of culture. For immunostaining, the cultures were fixed and stained for antibodies against human albumin (hepatocyte marker, green), CK8 (hepatocyte marker, red), and DAPI (nucleus, blue). Scale bar for panel B = 100 μm.

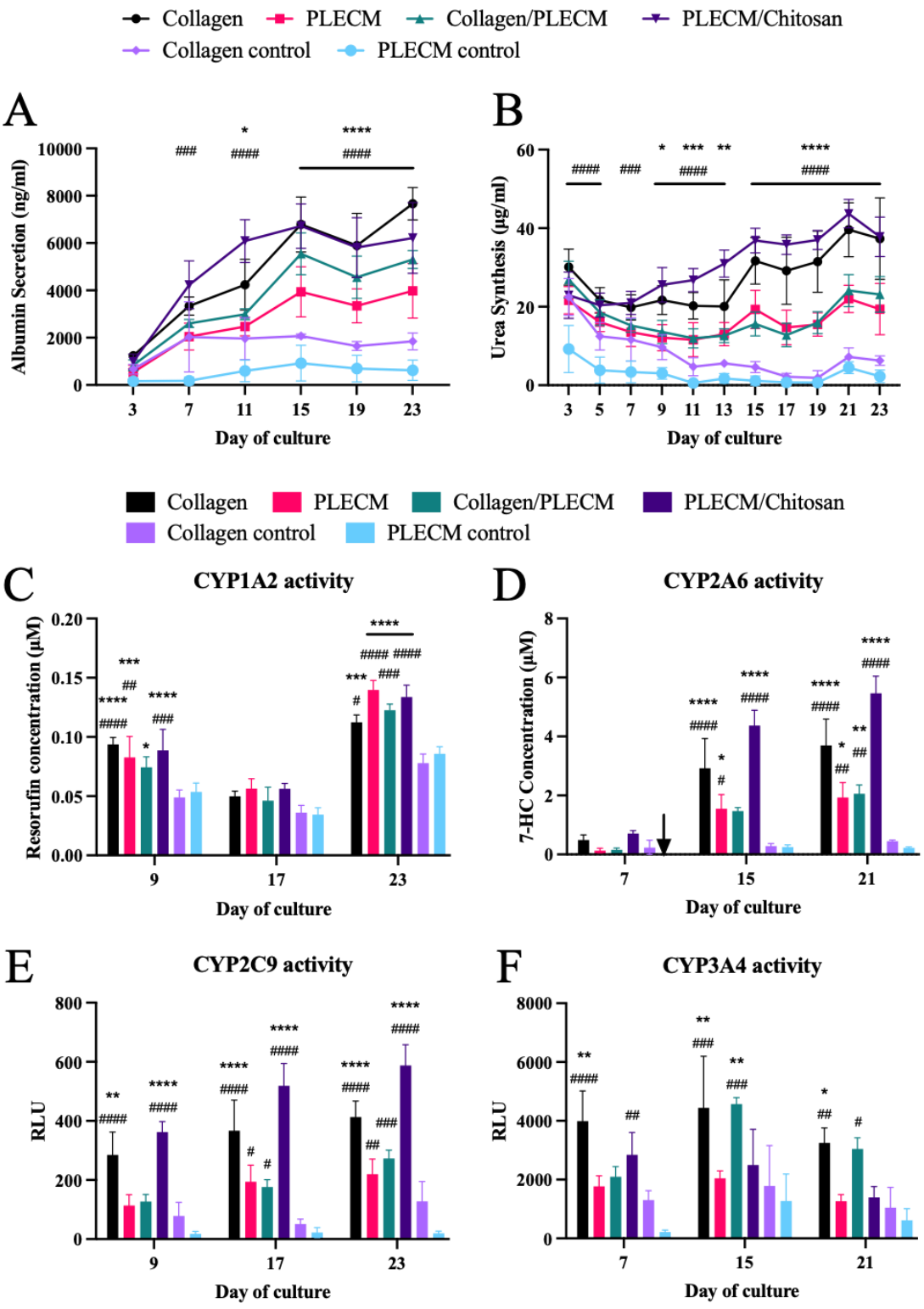

Figure 7: PHH/3T3-J2 co-culture functions on nanofibers and adsorbed ECM controls.

(A) Albumin secretion, (B) urea synthesis, (C) CYP1A2, (D) CYP2A6, (E) CYP2C9, and (F) CYP3A4 enzymes activities of PHH/3T3-J2 co-cultures on the nanofibers and adsorbed ECM

controls. Asterisks (*) indicate statistical significance relative to adsorbed collagen control and hash (#) indicates significance relative to adsorbed PLECM control. * or # p<.05, ** or ## p<.01, *** or ### p<.001, **** or #### p<.0001. Panels A and B show statistical comparisons for collagen-only nanofibers, while statistical comparisons for other nanofibers are shown in Supplemental Table 6.

References

[1] C.P. Monckton, G.E. Brown, S.R. Khetani, Latest impact of engineered human liver platforms on drug development, APL Bioeng 5(3) (2021) 031506.

[2] D.A. Kukla, S.R. Khetani, Bioengineered Liver Models for Investigating Disease Pathogenesis and Regenerative Medicine, Semin Liver Dis 41(3) (2021) 368-392.

[3] P. Godoy, N.J. Hewitt, U. Albrecht, M.E. Andersen, N. Ansari, S. Bhattacharya, J.G. Bode, J. Bolleyn, C. Borner, J. Böttger, A. Braeuning, R.A. Budinsky, B. Burkhardt, N.R. Cameron, G. Camussi, C.-S. Cho, Y.-J. Choi, J. Craig Rowlands, U. Dahmen, G. Damm, O. Dirsch, M.T. Donato, J. Dong, S. Dooley, D. Drasdo, R. Eakins, K.S. Ferreira, V. Fonsato, J. Fraczek, R. Gebhardt, A. Gibson, M. Glanemann, C.E.P. Goldring, M.J. Gómez-Lechón, G.M.M. Groothuis, L. Gustavsson, C. Guyot, D. Hallifax, S. Hammad, A. Hayward, D. Häussinger, C. Hellerbrand, P. Hewitt, S. Hoehme, H.-G. Holzhütter, J.B. Houston, J. Hrach, K. Ito, H. Jaeschke, V. Keitel, J.M. Kelm, B. Kevin Park, C. Kordes, G.A. Kullak-Ublick, E.L. LeCluyse, P. Lu, J. Luebke-Wheeler, A. Lutz, D.J. Maltman, M. Matz-Soja, P. McMullen, I. Merfort, S. Messner, C. Meyer, J. Mwinyi, D.J. Naisbitt, A.K. Nussler, P. Olinga, F. Pampaloni, J. Pi, L. Pluta, S.A. Przyborski, A. Ramachandran, V. Rogiers, C. Rowe, C. Schelcher, K. Schmich, M. Schwarz, B. Singh, E.H.K. Stelzer, B. Stieger, R. Stöber, Y. Sugiyama, C. Tetta, W.E. Thasler, T. Vanhaecke, M. Vinken, T.S. Weiss, A. Widera, C.G. Woods, J.J. Xu, K.M. Yarborough, J.G. Hengstler, Recent advances in 2D and 3D in vitro systems using primary hepatocytes, alternative hepatocyte sources and non-parenchymal liver cells and their use in investigating mechanisms of hepatotoxicity, cell signaling, and ADME., Archives of Toxicology 87(8) (2013) 1315-1530.

[4] D.R. Berger, B.R. Ware, M.D. Davidson, S.R. Allsup, S.R. Khetani, Enhancing the functional maturity of induced pluripotent stem cell-derived human hepatocytes by controlled presentation of cell-cell interactions in vitro., Hepatology 61(4) (2015) 1370-1381.

[5] P. Bedossa, V. Paradis, Liver extracellular matrix in health and disease., The Journal of pathology 200(4) (2003) 504-515.

[6] A. Sivaraman, J.K. Leach, S. Townsend, T. Iida, B.J. Hogan, D.B. Stolz, R. Fry, L.D. Samson, S.R. Tannenbaum, L.G. Griffith, A microscale in vitro physiological model of the liver: Predictive screens for drug metabolism and enzyme induction., Current Drug Metabolism 6(6) (2005) 569-591.

[7] S.R. Khetani, S.N. Bhatia, Microscale culture of human liver cells for drug development., Nature Biotechnology 26(1) (2008) 120-126.

[8] T.L. Sellaro, A. Ranade, D.M. Faulk, G.P. McCabe, K. Dorko, S.F. Badylak, S.C. Strom, Maintenance of human hepatocyte function in vitro by liver-derived extracellular matrix gels., Tissue Engineering, Part A 16(3) (2010) 1075-1082.

[9] G. Mattei, C. Magliaro, A. Pirone, A. Ahluwalia, Decellularized Human Liver Is Too Heterogeneous for Designing a Generic Extracellular Matrix Mimic Hepatic Scaffold, Artif Organs 41(12) (2017) E347-E355.

[10] C.P. Monckton, A. Brougham-Cook, K.B. Kaylan, G.H. Underhill, S.R. Khetani, Elucidating Extracellular Matrix and Stiffness Control of Primary Human Hepatocyte Phenotype Via Cell Microarrays, Adv Mater Interfaces 8(22) (2021).

[11] C. Frantz, K.M. Stewart, V.M. Weaver, The extracellular matrix at a glance, J Cell Sci 123(Pt 24) (2010) 4195-200.

[12] M. Ghaedi, M. Soleimani, I. Shabani, Y.Y. Duan, A.S. Lotfi, Hepatic differentiation from human mesenchymal stem cells on a novel nanofiber scaffold, Cellular & Molecular Biology Letters 17(1) (2012) 89-106.

[13] Z.-Q. Feng, M.K. Leach, X.-H. Chu, Y.-C. Wang, T. Tian, X.-L. Shi, Y.-T. Ding, Z.-Z. Gu, Electrospun chitosan nanofibers for hepatocyte culture., Journal of biomedical nanotechnology 6(6) (2010) 658-666.

[14] Z.Q. Feng, X.H. Chu, N.P. Huang, M.K. Leach, G. Wang, Y.C. Wang, Y.T. Ding, Z.Z. Gu, Rat hepatocyte aggregate formation on discrete aligned nanofibers of type-I collagen-coated poly(L-lactic acid), Biomaterials 31(13) (2010) 3604-3612.

[15] X.H. Chu, X.L. Shi, Z.Q. Feng, Z.Z. Gu, Y.T. Ding, Chitosan nanofiber scaffold enhances hepatocyte adhesion and function, Biotechnology Letters 31(3) (2009) 347-352.

[16] Z.Q. Feng, X.H. Chu, N.P. Huang, T. Wang, Y.C. Wang, X.L. Shi, Y.T. Ding, Z.Z. Gu, The effect of nanofibrous galactosylated chitosan scaffolds on the formation of rat primary hepatocyte aggregates and the maintenance of liver function, Biomaterials 30(14) (2009) 2753-2763.

[17] Y. Qiao, X. Liu, G. Fu, Z. He, C. Hou, Y. Li, Q. Zhang, H. Yan, H. Wang, An ordered electrospun polycaprolactone–collagen–silk fibroin scaffold for hepatocyte culture, Journal of Materials Science 53(3) (2017) 1623-1633.

[18] P. Das, M.D. DiVito, J.A. Wertheim, L.P. Tan, Collagen-I and fibronectin modified three-dimensional electrospun PLGA scaffolds for long-term in vitro maintenance of functional hepatocytes, Mater Sci Eng C Mater Biol Appl 111 (2020) 110723.

[19] P. Lin, W.C.W. Chan, S.F. Badylak, S.N. Bhatia, Assessing porcine liver-derived biomatrix for hepatic tissue engineering., Tissue engineering 10(7-8) (2004) 1046-1053.

[20] A. Kishen, S. Shrestha, A. Shrestha, C. Cheng, C. Goh, Characterizing the collagen stabilizing effect of crosslinked chitosan nanoparticles against collagenase degradation, Dent Mater 32(8) (2016) 968-77.

[21] S.D. Sarkar, B.L. Farrugia, T.R. Dargaville, S. Dhara, Chitosan-collagen scaffolds with nano/microfibrous architecture for skin tissue engineering, J Biomed Mater Res A 101(12) (2013) 3482-92.

[22] D. Rajendran, A. Hussain, D. Yip, A. Parekh, A. Shrirao, C.H. Cho, Long-term liver-specific functions of hepatocytes in electrospun chitosan nanofiber scaffolds coated with fibronectin, J Biomed Mater Res A 105(8) (2017) 2119-2128.

[23] P.C.F. da Câmara, L.Y.C. Madruga, R.M. Sabino, J. Vlcek, R.C. Balaban, K.C. Popat, A.F. Martins, M.J. Kipper, Polyelectrolyte multilayers containing a tannin derivative polyphenol improve blood compatibility through interactions with platelets and serum proteins, Materials Science and Engineering: C, Elsevier, 2020, p. 110919.

[24] R.M. Sabino, K. Kauk, L.Y.C. Madruga, M.J. Kipper, A.F. Martins, K.C. Popat, Enhanced hemocompatibility and antibacterial activity on titania nanotubes with tanfloc/heparin polyelectrolyte multilayers, J Biomed Mater Res A 108(4) (2020) 992-1005.

[25] L.Y.C. Madruga, R.C. Balaban, K.C. Popat, M.J. Kipper, Biocompatible Crosslinked Nanofibers of Poly(Vinyl Alcohol)/Carboxymethyl-Kappa-Carrageenan Produced by a Green Process, Macromolecular Bioscience 21 (2021) 2000292.

[26] L.Y.C. Madruga, K.C. Popat, R.C. Balaban, M.J. Kipper, Enhanced blood coagulation and antibacterial activities of carboxymethyl-kappa-carrageenan-containing nanofibers, Carbohydr Polym 273 (2021) 118541.

[27] L. Meng, O. Arnoult, M. Smith, G.E. Wnek, Electrospinning of in situ crosslinked collagen nanofibers, Journal of Materials Chemistry 22(37) (2012).

[28] G. Krishnamoorthy, R. Selvakumar, T.P. Sastry, S. Sadulla, A.B. Mandal, M. Doble, Experimental and theoretical studies on Gallic acid assisted EDC/NHS initiated crosslinked collagen scaffolds, Mater Sci Eng C Mater Biol Appl 43 (2014) 164-71.

[29] L.Y.C. Madruga, M.J. Kipper, Expanding the Repertoire of Electrospinning: New and Emerging Biopolymers, Techniques, and Applications, Adv Healthc Mater 11(4) (2022) e2101979.

[30] L.Y.C. Madruga, R.M. Sabino, E.C.G. Santos, K.C. Popat, R.C. Balaban, M.J. Kipper, Carboxymethyl-kappa-carrageenan: A study of biocompatibility, antioxidant and antibacterial activities, Int J Biol Macromol 152 (2020) 483-491.

[31] M.D. Davidson, S.R. Khetani, Intermittent Starvation Extends the Functional Lifetime of Primary Human Hepatocyte Cultures, Toxicol Sci 174(2) (2020) 266-277.

[32] X. Luo, Z. Guo, P. He, T. Chen, L. Li, S. Ding, H. Li, Study on structure, mechanical property and cell cytocompatibility of electrospun collagen nanofibers crosslinked by common agents, Int J Biol Macromol 113 (2018) 476-486.

[33] J. Burck, S. Heissler, U. Geckle, M.F. Ardakani, R. Schneider, A.S. Ulrich, M. Kazanci, Resemblance of electrospun collagen nanofibers to their native structure, Langmuir 29(5) (2013) 1562-72.

[34] A. Lončarević, M. Ivanković, A. Rogina, Lysozyme-Induced Degradation of Chitosan: The Characterisation of Degraded Chitosan Scaffolds, in: L. Ye (Ed.) Journal of Tissue Repair and Regeneration, 2017, pp. 12-22.

[35] U.M. Zanger, M. Schwab, Cytochrome P450 enzymes in drug metabolism: regulation of gene expression, enzyme activities, and impact of genetic variation, Pharmacol Ther 138(1) (2013) 103-41.

[36] S.S. Bale, I. Golberg, R. Jindal, W.J. McCarty, M.E. Luitje, M. Hegde, A. Bhushan, O.B. Usta, M.L. Yarmush, Long-term co-culture strategies for primary hepatocytes and liver sinusoidal endothelial cells, Tissue Engineering, Part C: Methods 21(4) (2015) 413-22.

[37] B.R. Ware, M.J. Durham, C.P. Monckton, S.R. Khetani, A Cell Culture Platform to Maintain Long-term Phenotype of Primary Human Hepatocytes and Endothelial Cells, Cell Mol Gastroenterol Hepatol 5(3) (2018) 187-207.

[38] S.R. Khetani, A.A. Chen, B. Ranscht, S.N. Bhatia, T-cadherin modulates hepatocyte functions in vitro., FASEB Journal 22(11) (2008) 3768-3775.

[39] S.R. Khetani, G. Szulgit, J.A. Del Rio, C. Barlow, S.N. Bhatia, Exploring interactions between rat hepatocytes and nonparenchymal cells using gene expression profiling., Hepatology 40(3) (2004) 545-554.

[40] R. Grant, J. Hallett, S. Forbes, D. Hay, A. Callanan, Blended electrospinning with human liver extracellular matrix for engineering new hepatic microenvironments, Sci Rep 9(1) (2019) 6293.

[41] R. Bual, H. Kimura, Y. Ikegami, N. Shirakigawa, H. Ijima, Fabrication of liver-derived extracellular matrix nanofibers and functional evaluation in in vitro culture using primary hepatocytes, Materialia 4 (2018) 518-528.

[42] A.F. Martins, S.P. Facchi, P.C.F. da Camara, S.E.A. Camargo, C.H.R. Camargo, K.C. Popat, M.J. Kipper, Novel poly(epsilon-caprolactone)/amino-functionalized tannin electrospun membranes as scaffolds for tissue engineering, J Colloid Interface Sci 525 (2018) 21-30.

[43] J. Almodóvar, M.J. Kipper, Coating Electrospun Chitosan Nanofibers with Polyelectrolyte Multilayers Using the Polysaccharides Heparin and N,N,N-Trimethyl Chitosan, Macromolecular bioscience 11(1) (2011) 72-76.

[44] T.T. Ruckh, K. Kumar, M.J. Kipper, K.C. Popat, Osteogenic differentiation of bone marrow stromal cells on poly(epsilon-caprolactone) nanofiber scaffolds, Acta Biomater 6(8) (2010) 2949-59.

[45] S.V. Shilova, A.Y. Tret'yakova, V.P. Barabanov, Association of Chitosan in Aqueous-Alcohol Solutions, Polymer Science, Series A 60 (2018) 184-189.

[46] S.S. Desai, J.C. Tung, V.X. Zhou, J.P. Grenert, Y. Malato, M. Rezvani, R. Espanol-Suner, H. Willenbring, V.M. Weaver, T.T. Chang, Physiological ranges of matrix rigidity modulate primary mouse hepatocyte function in part through hepatocyte nuclear factor 4 alpha, Hepatology 64(1) (2016) 261-75.

[47] S. Mueller, L. Sandrin, Liver stiffness: a novel parameter for the diagnosis of liver disease, Hepat Med 2 (2010) 49-67.

[48] R.E. Coronado, M. Somaraki-Cormier, S. Natesan, R.J. Christy, J.L. Ong, G.A. Halff, Decellularization and Solubilization of Porcine Liver for Use as a Substrate for Porcine Hepatocyte Culture: Method Optimization and Comparison, Cell Transplant 26(12) (2017) 1840-1854.

[49] B. Tarus, N. Fadel, A. Al-Oufy, M. El-Messiry, Effect of polymer concentration on the morphology and mechanical characteristics of electrospun cellulose acetate and poly (vinyl chloride) nanofiber mats, Alexandria Engineering Journal 55 (2016) 2975-2984.

[50] S.S.S. Bakar, K.M. Foong, N.A. Halif, S. Yahud, Effect of solution concentration and applied voltage on electrospun polyacrylonitrile fibers, IOP Conference Series: Materials Science and Engineering 701 (2019) 012018.

[51] J. Fan, Y. Shang, Y. Yuan, J. Yang, Preparation and characterization of

chitosan/galactosylated hyaluronic acid scaffolds for primary hepatocytes culture, J Mater Sci Mater Med 21(1) (2010) 319-27.

[52] A. Stampella, A. Papi, G. Rizzitelli, M. Costantini, C. Colosi, A. Barbetta, M. Massimi, L.C. Devirgiliis, M. Dentini, Synthesis and characterization of a novel poly(vinyl alcohol) 3D platform for the evaluation of hepatocytes' response to drug administration, J Mater Chem B 1(24) (2013) 3083-3098.

[53] C.S. Ranucci, A. Kumar, S.P. Batra, P.V. Moghe, Control of hepatocyte function on collagen foams: sizing matrix pores toward selective induction of 2-D and 3-D cellular morphogenesis, Biomaterials 21(8) (2000) 783-93.

[54] R.J. Schulze, M.B. Schott, C.A. Casey, P.L. Tuma, M.A. McNiven, The cell biology of the hepatocyte: A membrane trafficking machine, J Cell Biol (2019).

[55] C.M. Brophy, J.L. Luebke-Wheeler, B.P. Amiot, R.P. Remmel, P. Rinaldo, S.L. Nyberg, Gene expression and functional analyses of primary rat hepatocytes on nanofiber matrices, Cells Tissues Organs 191(2) (2010) 129-40.

[56] C.M. Brophy, J.L. Luebke-Wheeler, B.P. Amiot, H. Khan, R.P. Remmel, P. Rinaldo, S.L. Nyberg, Rat hepatocyte spheroids formed by rocked technique maintain differentiated hepatocyte gene expression and function, Hepatology 49(2) (2009) 578-86.

[57] T.V. Nguyen, O. Ukairo, S.R. Khetani, M. McVay, C. Kanchagar, W. Seghezzi, G. Ayanoglu, O. Irrechukwu, R. Evers, Establishment of a hepatocyte-Kupffer cell coculture model for assessment of proinflammatory cytokine effects on metabolizing enzymes and drug transporters., Drug Metabolism and Disposition 43(5) (2015) 774-785.

[58] M.D. Davidson, D.A. Kukla, S.R. Khetani, Microengineered cultures containing human hepatic stellate cells and hepatocytes for drug development, Integrative Biology 9(8) (2017) 662-677.

[59] W.W. Wang, S.R. Khetani, S. Krzyzewski, D.B. Duignan, R.S. Obach, Assessment of a micropatterned hepatocyte coculture system to generate major human excretory and circulating drug metabolites, Drug Metabolism and Disposition 38(10) (2010) 1900-1905.

[60] S.R. Khetani, C. Kanchagar, O. Ukairo, S. Krzyzewski, A. Moore, J. Shi, S. Aoyama, M. Aleo, Y. Will, Use of micropatterned cocultures to detect compounds that cause drug-induced liver injury in humans., Toxicological Sciences 132(1) (2013) 107-117.

[61] A. Shlomai, R.E. Schwartz, V. Ramanan, A. Bhatta, Y.P. de Jong, S.N. Bhatia, C.M. Rice, Modeling host interactions with hepatitis B virus using primary and induced pluripotent

stem cell-derived hepatocellular systems., Proceedings of the National Academy of Sciences 111(33) (2014) 12193-12198.

[62] S. March, S. Ng, S. Velmurugan, A. Galstian, J. Shan, D.J. Logan, A.E. Carpenter, D. Thomas, B.K.L. Sim, M.M. Mota, S.L. Hoffman, S.N. Bhatia, A microscale human liver platform that supports the hepatic stages of Plasmodium falciparum and vivax., Cell Host & Microbe 14(1) (2013) 104-115.

[63] M.D. Davidson, K.R. Ballinger, S.R. Khetani, Long-term exposure to abnormal glucose levels alters drug metabolism pathways and insulin sensitivity in primary human hepatocytes., Scientific Reports 6 (2016) 28178.